

~~CONFIDENTIAL~~

30 APR 1946

~~CLASSIFICATION
HANDLED TO RESTRICTED~~**NACA**

RESEARCH MEMORANDUM

HIGH-SPEED STABILITY AND CONTROL CHARACTERISTICS

OF A FIGHTER AIRPLANE MODEL WITH A
SWEPT-BACK WING AND TAIL

By Charles P. Morrill, Jr. and Lee E. Beatty

Ames Aeronautical Laboratory
Moffett Field, Calif.~~CLASSIFICATION CHANGED~~

To

~~Confidential~~
CO 10501

NACA RF 2179

By authority of

J. W. Crowley

CLASSIFIED DOCUMENT

Date 12-14-54

H--1-15-54

This document contains classified information affecting the National Defense of the United States within the meaning of the Espionage Act, USC 5032 and 5042. Its transmission or the revelation of its contents in any manner to an unauthorized person is prohibited by law. Information so classified may be imparted only to persons in the military and naval services of the United States, appropriate civilian officers and employees of the Federal Government who have a legitimate interest therein, and to United States citizens of known loyalty and discretion who of necessity must be informed thereof.

CLASSIFICATION CANCELED

Authority NACA RF 3147 Date 11/14/55

By 22124-1249/55 Sec

NATIONAL ADVISORY COMMITTEE FOR AERONAUTICS

WASHINGTON
April 14, 1946

NACA LIBRARY

LANGLEY MEMORIAL AERONAUTICAL
LABORATORY
Langley Field, Va.~~CONFIDENTIAL~~~~CONFIDENTIAL~~



3 1176 01434 4452

NATIONAL ADVISORY COMMITTEE FOR AERONAUTICS

RESEARCH MEMORANDUM

HIGH-SPEED STABILITY AND CONTROL CHARACTERISTICS

OF A FIGHTER AIRPLANE MODEL WITH A

SWEPT-BACK WING AND TAIL

By Charles P. Morrill, Jr. and Lee E. Boddy

SUMMARY

The results of wind-tunnel tests conducted to determine the high-speed stability and control characteristics of an airplane model with a swept-back wing and tail are presented in this report. There are included the aerodynamic coefficients and the longitudinal- and lateral-control characteristics of the plain wing-fuselage-tail combination. Also included are the effects of wing leading-edge slats and fuselage-side dive brakes.

Divergence of the drag occurred at approximately 0.86 Mach number and was accompanied by an increase in static longitudinal stability. However, no uncontrollable tendency to pitch down at high speeds was noted. The leading-edge slats proved effective in delaying the stall and instability at high lift coefficients but caused longitudinal instability at low lift coefficients and high Mach numbers. Each 10° deflection of the dive brakes increased the drag coefficient approximately 0.007 and increased the pitching-moment coefficient about the same amount as a 0.7° upward elevator deflection.

INTRODUCTION

This report presents the high-speed stability and control characteristics of a fighter airplane model with a 35° swept-back wing and tail. The data presented herein were obtained from tests made in the Ames 16-foot high-speed wind tunnel of a semispan model of the airplane. For results of other tests conducted with the same model, consult references 1 and 2 which cover modifications to the original model and the effects of external stores, respectively.

~~CONFIDENTIAL~~**CONFIDENTIAL**

The high-speed data contained in this report included the basic aerodynamic characteristics of the model, the effectiveness and hinge-moment characteristics of the control surfaces, the effect of wing leading-edge slats, and the effect of the fuselage-side dive brakes.

SYMBOLS

The symbols used in this report are defined as follows:

R	Reynolds number
M	Mach number
α	angle of attack of fuselage reference line, degrees
C_L	lift coefficient $\left(\frac{\text{twice lift of half model}}{qS} \right)$
C_D	drag coefficient $\left(\frac{\text{twice drag of half model}}{qS} \right)$
C_m	pitching-moment coefficient $\left(\frac{\text{twice pitching moment of half model}}{qS \text{ M.A.C.}} \right)$
δ_e	elevator deflection about hinge line, degrees
i_t	stabilizer incidence relative to fuselage reference line, degrees
C_{h_e}	elevator hinge-moment coefficient $\left(\frac{\text{twice elevator hinge moment of half model}}{q b_e c_e^2} \right)$
C_{h_t}	stabilizer hinge-moment coefficient $\left(\frac{\text{twice stabilizer hinge moment of half model}}{q S_t \text{ M.A.C.}_t} \right)$
F_s	stick force, pounds $\left(C_{h_e} q b_e \overline{c_e^2} \times \frac{\delta_e}{\delta_{e1s}} \right)$
C_l	rolling-moment coefficient $\left(\frac{\text{rolling moment of half model}}{qSb} \right)$
δ_a	aileron deflection about hinge line, degrees

~~CONFIDENTIAL~~

C_{h_a} aileron hinge-moment coefficient $\left(\frac{\text{aileron hinge moment}}{q b_a c_a^2} \right)$

δ_B fuselage-side dive-brake inner-door deflection, degrees

where

q free-stream dynamic pressure, pounds per square foot

S twice wing area of half model, square feet

M.A.C. mean aerodynamic chord of wing, feet

b twice the wing semispan, feet

b_e twice elevator hinge-line length, feet

$\overline{c_e^2}$ mean square chord of elevator normal to hinge line, square feet

S_t twice horizontal tail area of half model, square feet

M.A.C._t mean aerodynamic chord of horizontal tail, feet

δ_s stick deflection, degrees

l_s stick length, feet

b_a aileron hinge-line length, feet

$\overline{c_a^2}$ mean square chord of aileron normal to hinge line, square feet

MODEL AND APPARATUS

A semispan, 0.20-scale model of a fighter airplane with 35° swept-back wing and tail was employed in these tests, which were conducted in the Ames 16-foot high-speed wind tunnel. The half model was mounted on the trunnion of the wind-tunnel balance frame with its center plane approximately 6 inches from the tunnel wall as shown in figure 1. A steel separation plate fastened to the turntable in the tunnel wall by means of a fairing served as a reflection plane for the half model. (See reference 1 for sketch and more detailed description of the installation.)

The model was tested without canopy, dorsal fin, or vertical tail. The horizontal tail was not equipped with trim tabs but the stabilizer was designed for variable incidence.

The wing of the model had a leading-edge slat of constant chord (24 percent of wing chord at the outboard end and 15 percent at the inboard end measured parallel to the center line) as shown in figure 2. The inboard end of the slat was 10.82 inches from the fuselage center line. The span of the slat was 31.05 inches (69 percent of the wing semispan) measured normal to the center line; and the chord was 3.29 inches measured parallel to the center line. Brackets of various lengths were used to fasten the slat to the wing in the closed, one-quarter extended, one-half extended, or fully extended position. The maximum extension was 1.461 inches normal to the wing leading edge, the chordwise extension then being 10.7 percent at the outboard end and 6.7 percent at the inboard end measured parallel to the center line. The maximum extension was accompanied by a tilt or droop of the slat $9^{\circ} 36'$ below the wing reference plane. For intermediate extensions the droop was proportionally smaller.

A dive brake of the folding-door type was incorporated in the side of the fuselage. (See fig. 3.) The inner door pivoted about a hinge line at fuselage station 65.2. The combined area of both doors of the brake was 0.298 square feet (4.3 percent of the wing area of the half model) and the chord of the inner door was 0.471 feet. In addition to the normally closed position the dive brake could be deflected 20° , 40° , or 85° , the angle being measured between the inner door and its closed position.

Pertinent model dimensions are:

Wing

Area (whole model), sq ft	11.516
Span (whole model), ft	7.423
Aspect ratio	4.785
Taper ratio	0.513
Dihedral, deg	3.0
Mean aerodynamic chord, ft	1.617
Sweepback of 25-percent-chord line, deg	35.22
Root incidence, deg	1.0
Tip incidence, deg	-1.0

Root airfoil section¹ modified NACA 0012-64

Tip airfoil section¹ modified NACA 0011-64

Aileron (one only)

Area (aft of hinge line), sq ft 0.746

Span, ft 2.008

Mean square chord, sq ft 0.154

Horizontal Tail

Area (whole model), sq ft 1.400

Span (whole model) ft 2.550

Aspect ratio 4.650

Taper ratio 0.450

Dihedral, deg 10.0

Mean aerodynamic chord, ft 0.578

Sweepback of 25-percent-chord line, deg 35.59

Airfoil section (parallel to
center line) NACA 0010-64

Elevator

Area (whole model), sq ft 0.405

Span (whole model), ft 2.310

Mean square chord, sq ft 0.0248

Stabilizer

Area (whole model), sq ft 0.995

Span (whole model), ft 2.550

¹Both sections taken normal to 25-percent-chord line. (See reference 1 for details on modification to section.)

TESTS

The investigation consisted of a determination of the general characteristics of the half model and a study of the effects of the wing leading-edge slats and the fuselage dive brakes on these characteristics. As indicated in the definitions of symbols, the data have been modified to apply to a whole model and the discussion following will be on the basis of a complete model.

The slats were tested in the closed, one-quarter extended, one-half extended, and fully extended positions. Data were obtained for dive brake deflections of 0° , 20° , 40° , and 85° .

The test Reynolds number, based on the mean aerodynamic chord of the wing, varied from 3.35 million at 0.30 Mach number to 6.20 million at a Mach number of 0.90. (See fig. 4.)

Pitching moments are referred to a center 2.68 inches above the 25-percent point of the mean aerodynamic chord of the wing (fuselage station 37.70). The horizontal-tail hinge moments are given about a hinge axis 1.44 inches below the 4.3-percent point of the mean aerodynamic chord of the tail.

No tare corrections have been applied to the data since no part of the support system was exposed to the main air stream. The effects of the wind-tunnel walls on the angle of attack, drag, and pitching moment have not been accounted for since they are small for a model of this size and, in general, have the opposite effect of the leakage. Also, no correction has been applied to the aileron effectiveness to account for the end-plate effect of the reflection plane. The aileron effectiveness of the half model agreed well with that obtained from preliminary tests of the whole model mounted in the center of the wind tunnel. However, constriction effects of the model and support system have been taken into account. Since the model was small relative to the test section the constriction correction to the Mach number was less than 2 percent at 0.90 Mach number.

The magnitude of the drag coefficients appears to be too large due to the effects of leakage air passing over the supporting structure inside the fairing. However, the variation of drag with Mach number is believed to be reliable.

RESULTS AND DISCUSSION

Figure 4 gives the average variation of Reynolds number with Mach number during the tests. The basic characteristics of the model are presented in figures 5 through 8. Longitudinal and lateral

characteristics for zero yaw together with accompanying control-surface hinge moments are given in figures 9 through 16. Figures 17 to 21 present the effect of the wing slats; and data on the dive brake are given in figures 22 through 25.

Lift, Drag, and Pitching Moment

The variation of lift coefficient with angle of attack and Mach number is presented in figure 5. The average slope of the lift curve increased with increasing Mach number, but the angle of attack for zero lift remained essentially constant up to 0.90 Mach number.

At low lift coefficients the drag coefficients remained relatively constant to a Mach number of about 0.86, at which divergence occurred. At higher lift coefficients the divergence Mach number was lowered to approximately 0.825. (See fig. 6.)

The variation of pitching-moment coefficient with lift coefficient of the model with the horizontal tail removed indicated longitudinal instability at Mach numbers up to approximately 0.85, at which the model became neutrally stable. (See fig. 7.) At higher Mach numbers the model exhibited stable characteristics. The pitching-moment coefficient at zero lift showed only slight variation within the limits of the test (-0.008 to 0.003). Pitching-moment characteristics of the model with the horizontal tail (fig. 8) indicated static longitudinal stability for moderate lift coefficients at all test Mach numbers. However, a strong tendency existed for the model to become longitudinally unstable at the higher lift coefficients, especially with a negative deflection of the elevator or stabilizer.

Longitudinal Characteristics

Figure 9 presents the variation of lift- and pitching-moment-curve slopes with Mach number. At low lift coefficients the lift-curve slope increased gradually with Mach number. The curve for 0.4 lift coefficient shows a decrease of slope from low to medium Mach numbers followed by a gradual increase, reaching a peak at 0.85 Mach number and decreasing rapidly thereafter.

The static instability exhibited below 0.85 Mach number by the model without the horizontal tail increased considerably at lift coefficients greater than 0.4. However, adding the tail restored stability for moderate lift coefficients at all Mach numbers within

the test limits. At lift coefficients above about 0.4 the degree of stability was appreciably reduced. At a Mach number of 0.85 the longitudinal stability at zero lift began to increase; however, the actual magnitude of the stability derivative did not exceed controllable limits up to a Mach number of 0.90.

The approximate variation of elevator and stabilizer effectiveness with Mach number is shown in figure 10. Inconsistencies in the data prevented more detailed and accurate evaluation of these parameters. However, the curves presented are believed to be representative of the characteristics of these control surfaces.

The slope of the elevator-hinge-moment curves (fig. 11) increased with Mach number for large elevator deflections but decreased for small deflections. At small deflections there was a tendency toward overbalance which actually occurred at a Mach number of 0.875 with zero stabilizer incidence and an angle of attack of 4° . While data for 4° angle of attack at 0.90 Mach number are not available, indications are that overbalance would have occurred. Little change in elevator hinge-moment coefficient with change in stabilizer incidence was noticeable below about 0.85 Mach number.

Figure 12 presents the variation of stabilizer hinge-moment coefficient with elevator deflection. The variations of hinge-moment coefficient with both angle of attack and Mach number were relatively constant within the range of the test. The variation of stabilizer hinge-moment coefficient with stabilizer incidence is shown in figure 13.

The elevator angles required for level flight were calculated with an assumed gross weight of 13,100 pounds. These deflections together with the stick forces required to maintain balance at several altitudes and zero stabilizer incidence are shown in figure 14. Since the stabilizer effectiveness was approximately 2 to 3 times that of the elevator, it is apparent that the stabilizer was sufficiently effective to trim the model at all speeds included in the range of the test.

Lateral Characteristics

As indicated by figure 15, the aileron effectiveness remained essentially constant between Mach numbers of 0.3 and 0.90, although there was some indication of reduced effectiveness at the higher angles of attack at a Mach number of 0.90. At all other Mach numbers within the range of the tests the effect of increasing the angle of

attack was noticeable but not serious. Figure 16 presents the aileron hinge-moment coefficients.

Wing Leading-Edge Slats

The lift characteristics of the model for several positions of the leading-edge slat are shown in figure 17. The effect of delaying the stall at high lift coefficients is clearly apparent at low Mach numbers. At a Mach number of 0.30 the extended slats increased the lift coefficient at which stall occurred about 0.25. At small angles of attack the extended slats reduced the lift coefficient slightly. However, this effect is diminished as the angle of attack is increased and is reversed at high angles.

At low lift coefficients the extended slats also caused an increase in the drag coefficient of about 0.015 to 0.020. However, because the extended slats delayed the stall, the drag coefficients at high lift coefficients were smaller with the slats extended. The increment of drag caused by the extended slats at low lift coefficients remained essentially constant with Mach number. (See fig. 18.)

Figures 19 and 20 show the effect of the slats on the pitching-moment characteristics of the model. At low Mach numbers, the fully extended slat alleviated the tip stall encountered with the slat retracted, so that at the maximum lift coefficient the model was longitudinally stable. However, for a small range of lift coefficients immediately below the stall the model exhibited a tendency for instability even with the slat extended. Extension of the slats at Mach numbers above 0.80 and lift coefficients below 0.20 resulted in serious loss of static longitudinal stability.

Figure 21 presents the effect of the slats on the aileron effectiveness. In general, the slats decreased the effectiveness of the aileron for upward deflections and increased it for downward deflections. The effect was small in both cases. There is some indication that the intermediate positions of the slats caused greater loss than the extended positions.

Fuselage-Side Dive Brakes

Extending the fuselage dive brakes produced negligible effect on the lift of the model. (See fig. 22.)

The increase in drag coefficient due to the dive brakes amounted to about 0.007 for each 10° deflection of the brake and increased only slightly with Mach number. (See fig. 23.)

Figure 24 shows that the dive brakes supplied a positive pitching-moment increment to the model approximately equal in effect to 0.7° of elevator deflection for each 10° of brake deflection, giving a maximum effect comparable to about 6° of upward elevator deflection with the brake completely extended. No important effect on the static longitudinal stability was noted.

The effectiveness of the elevator was reduced approximately 35 percent with the dive brakes deflected 85° , as indicated in figure 25. The percentage loss in effectiveness remained relatively constant with Mach number. (Discretion should be employed in the use of fig. 25 as the limited amount of data obtained was somewhat erratic.)

CONCLUSIONS

The following conclusions may be drawn from the preceding discussion:

1. At low lift coefficients divergence of the drag occurred at a Mach number of approximately 0.86.
2. The model exhibited no uncontrollable tendency to nose down at Mach numbers within the limits of the tests (0.30 to 0.90).
3. Static longitudinal stability began to increase at a Mach number of about 0.85 but did not exceed controllable limits within the range of the tests.
4. The extended wing-leading-edge slats cause longitudinal instability at low lift coefficients and high Mach numbers but were otherwise effective in delaying the stall at high angles of attack and preventing instability at high lift coefficients.
5. Each 10° deflection of the fuselage-side dive brakes supplied a drag-coefficient increment of about 0.007 and an increment of positive pitching moment about equal that produced by 0.7° upward elevator deflection.

6. The effectiveness of the elevator was reduced about 35 percent with the dive brakes deflected 85° .

Ames Aeronautical Laboratory,
National Advisory Committee for Aeronautics,
Moffett Field, Calif.

REFERENCES

1. Boddy, Lee E., and Morrill, Charles P., Jr.: The Aerodynamic Effects of Modifications to the Wing and Wing-Fuselage Intersection of an Airplane Model with the Wing Swept Back 35° . NACA CRM No. A7J02, 1947.
2. Boddy, Lee E., and Morrill, Charles P., Jr.: The Aerodynamic Effects of Rockets and Fuel Tanks Mounted Under the Swept-Back Wing of an Airplane Model. NACA CRM No. A7J03, 1947.

•

•

•

•

•

•



(a) Three-quarter front view.



(b) Side view.

Figure 1.- Semispan model mounted in wind tunnel.

4

5

6

7

8

9

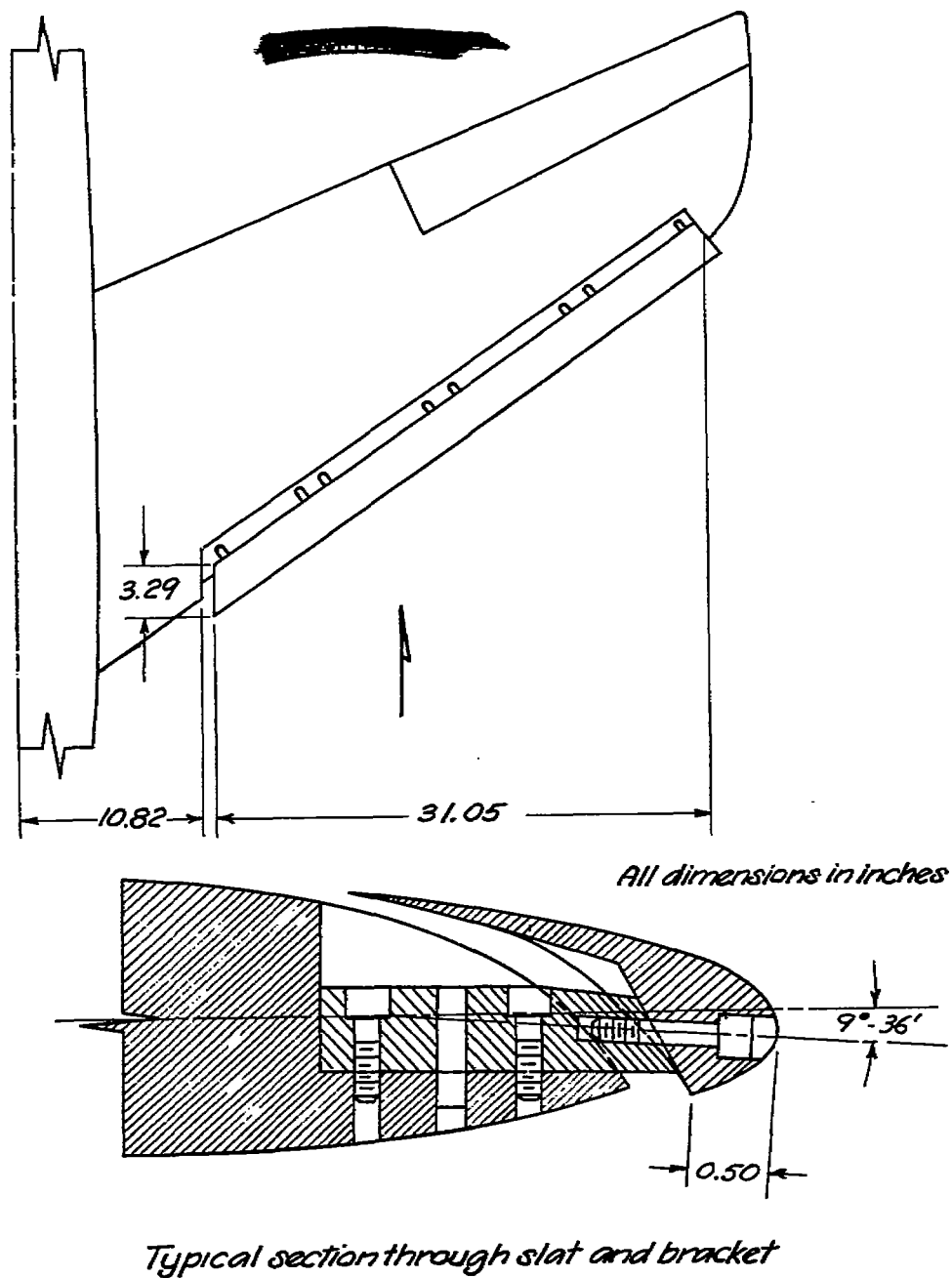


Figure 2.- Plan and detail of wing-leading-edge slat

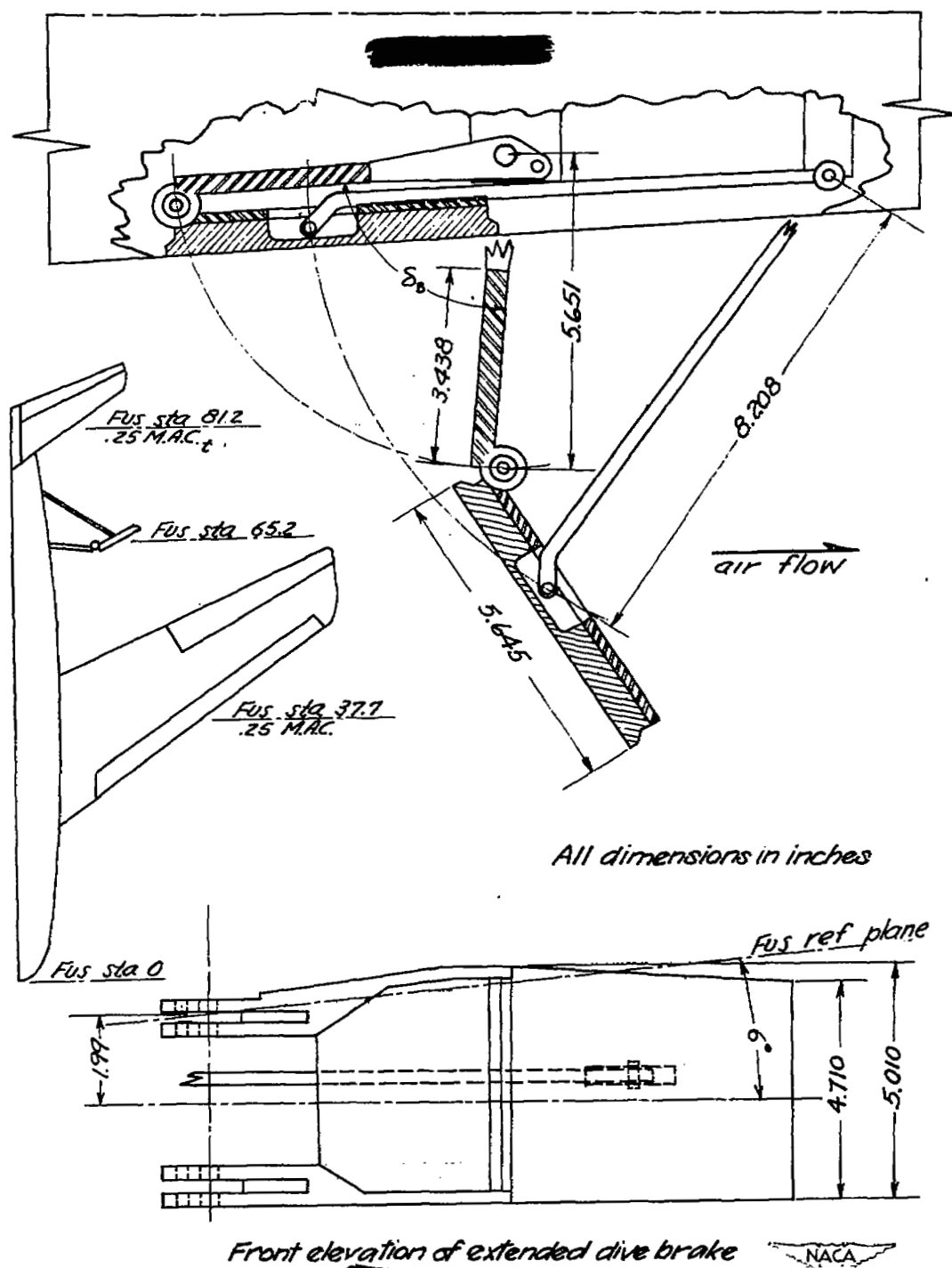


Figure 3.- Plan and detail of fuselage-side dive brake

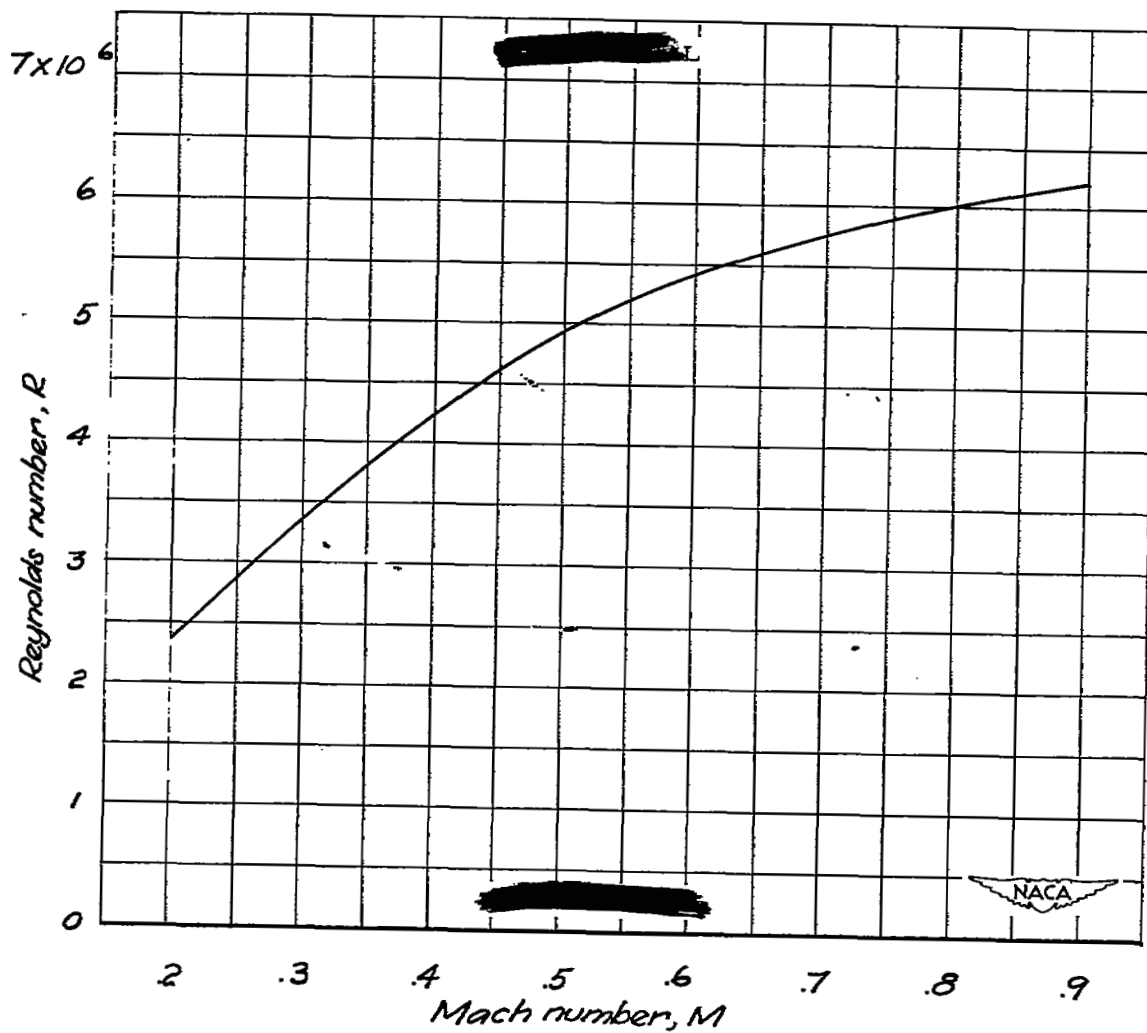


Figure 4.- Average variation of Reynolds number with Mach number

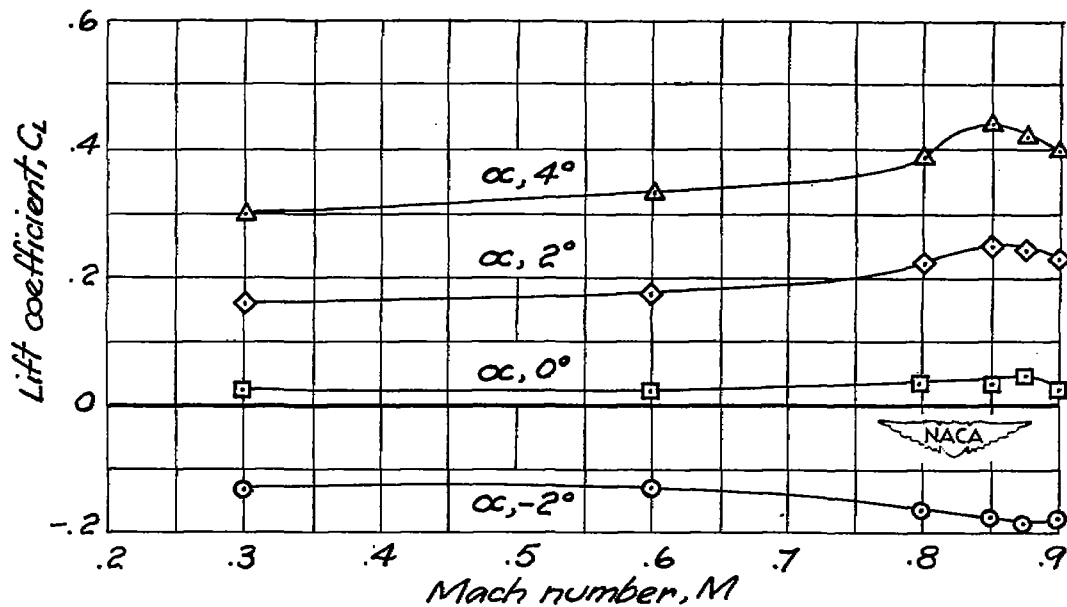
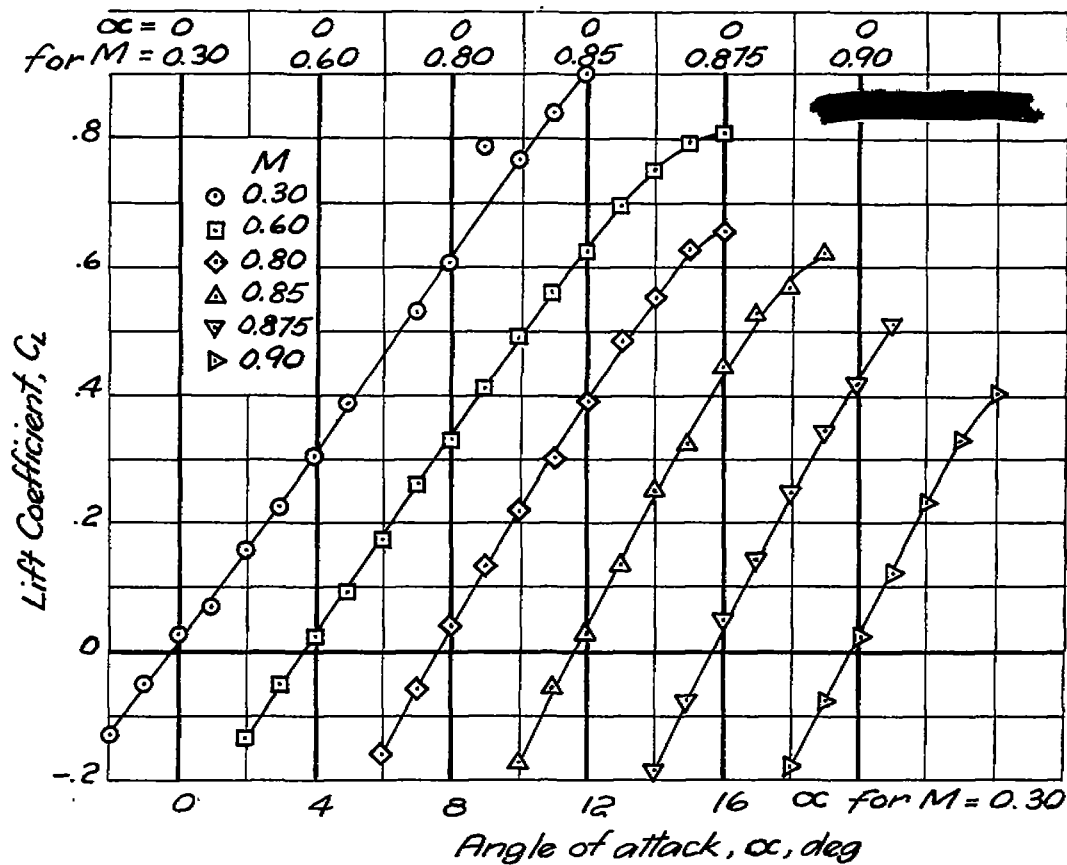


Figure 5.- Lift characteristics of the model

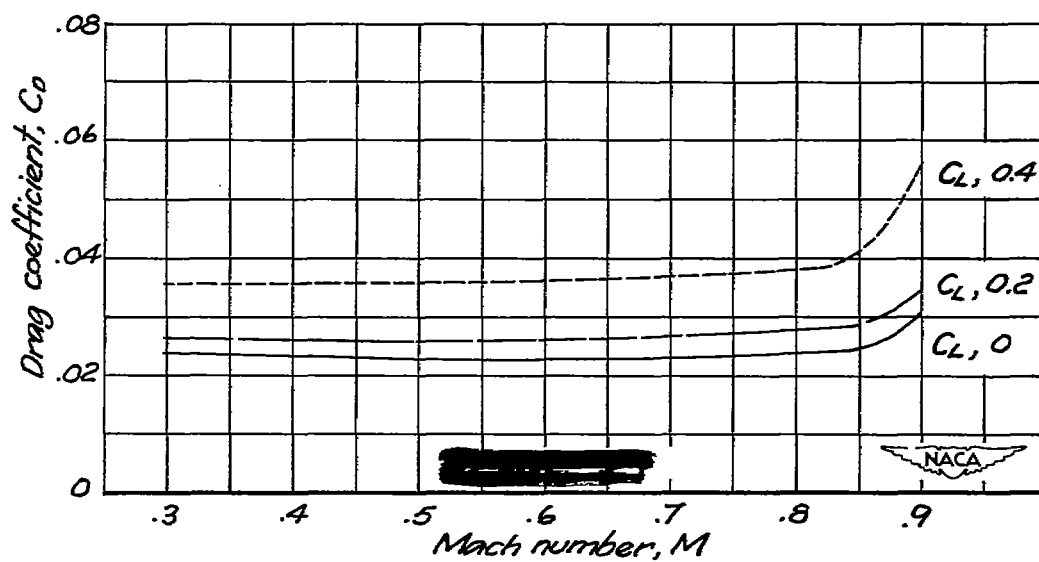
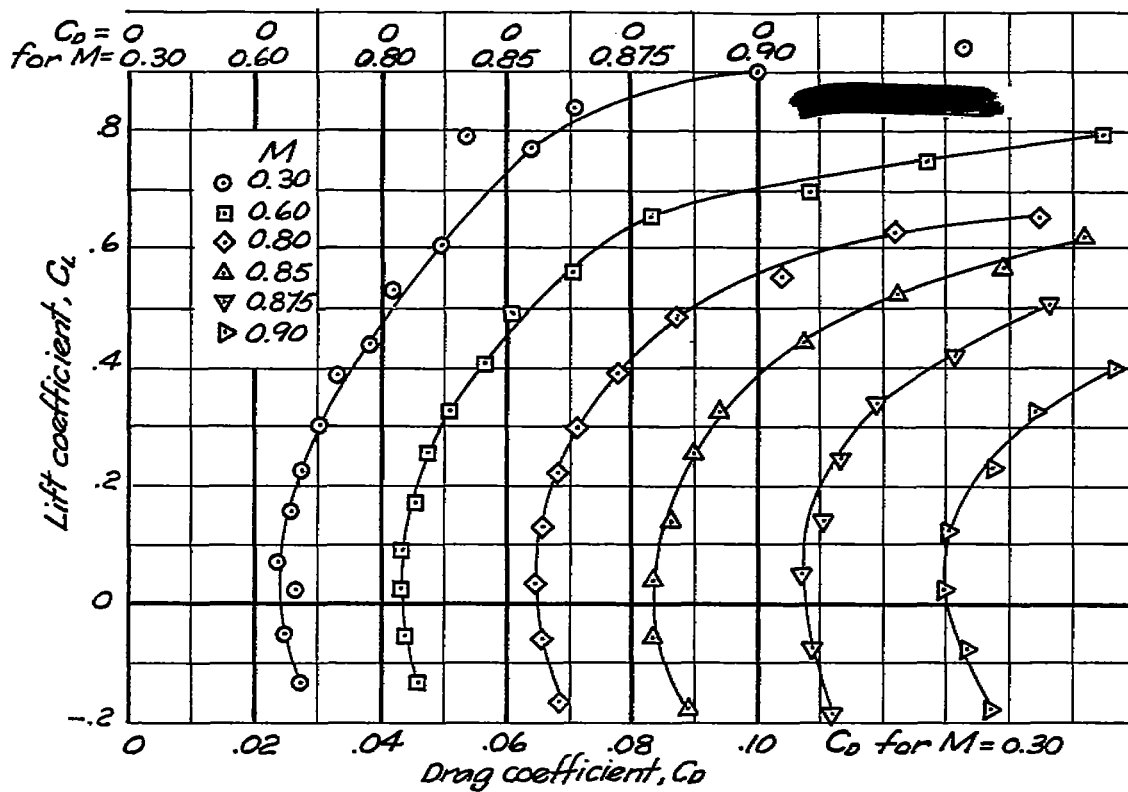


Figure 6. - Drag characteristics of the model

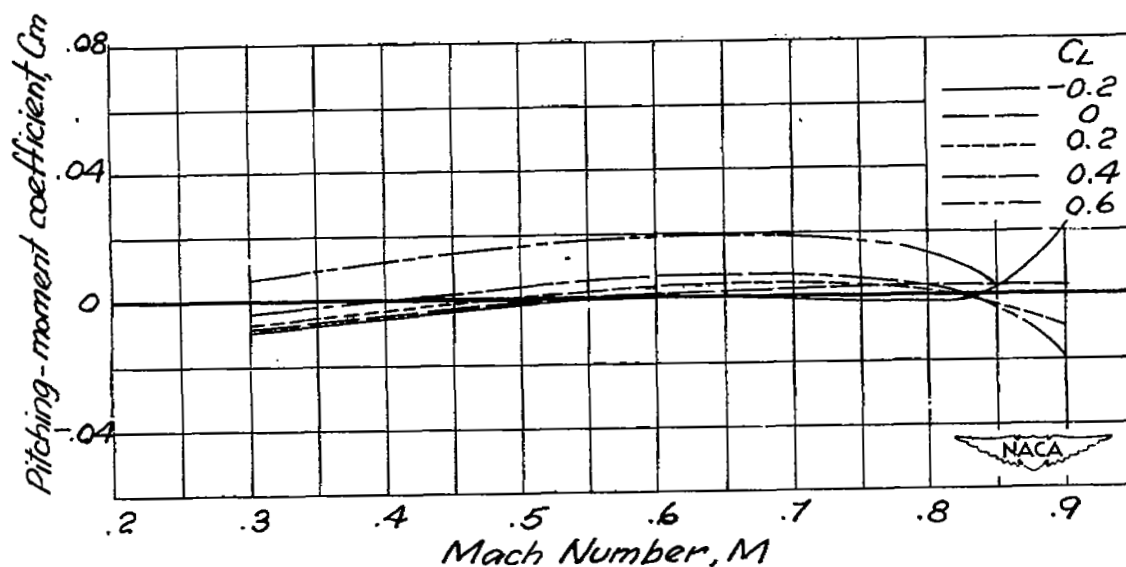
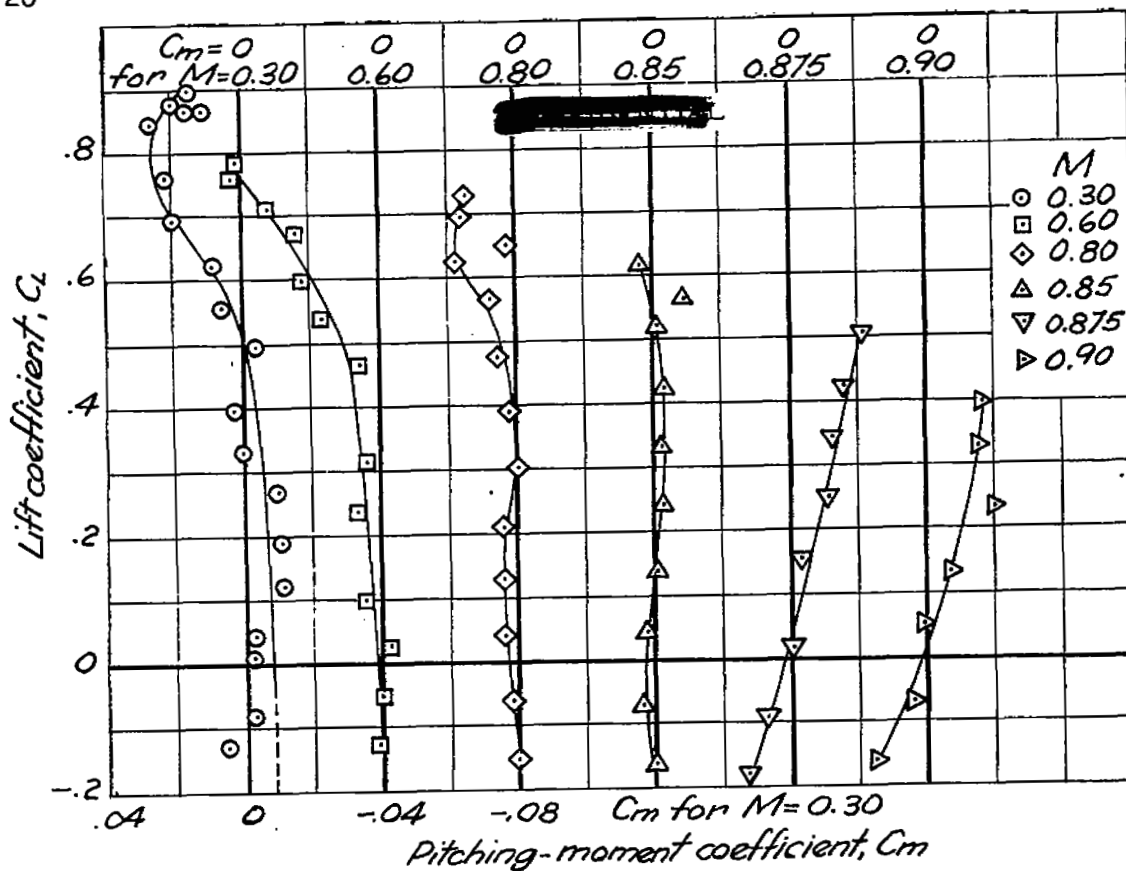
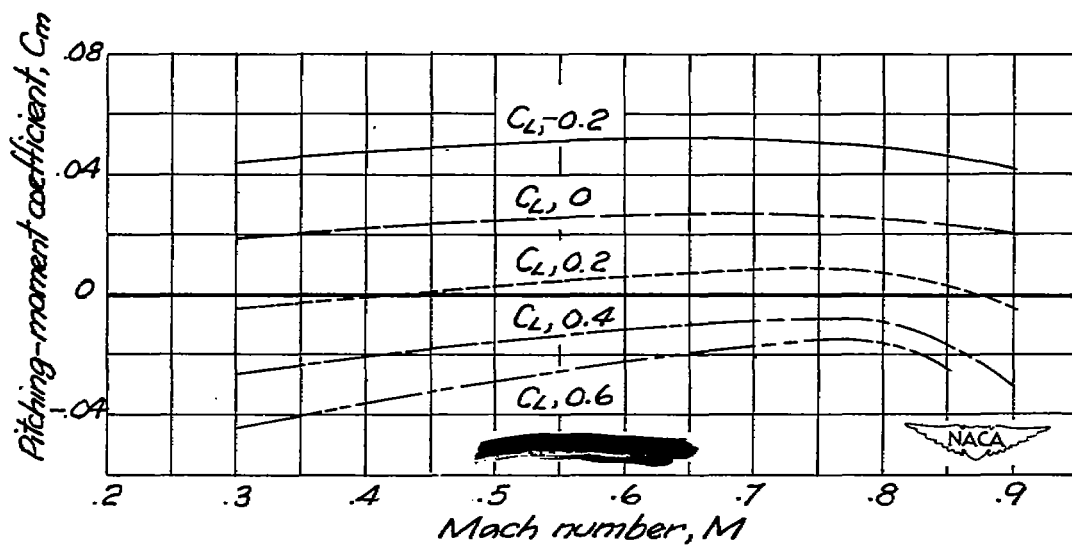
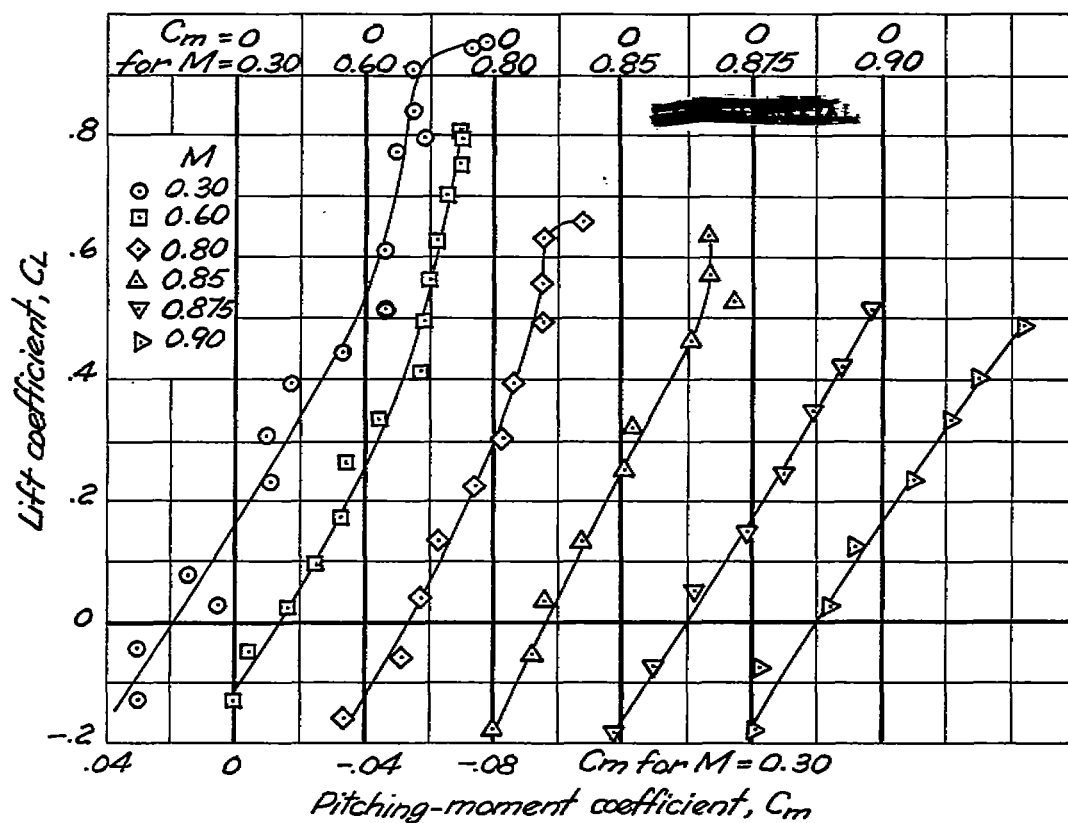
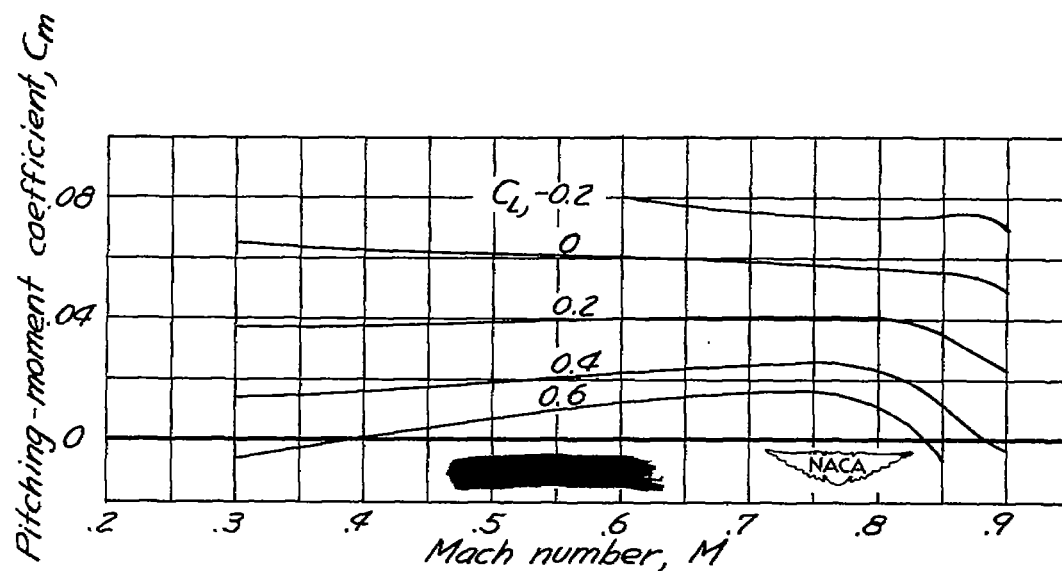
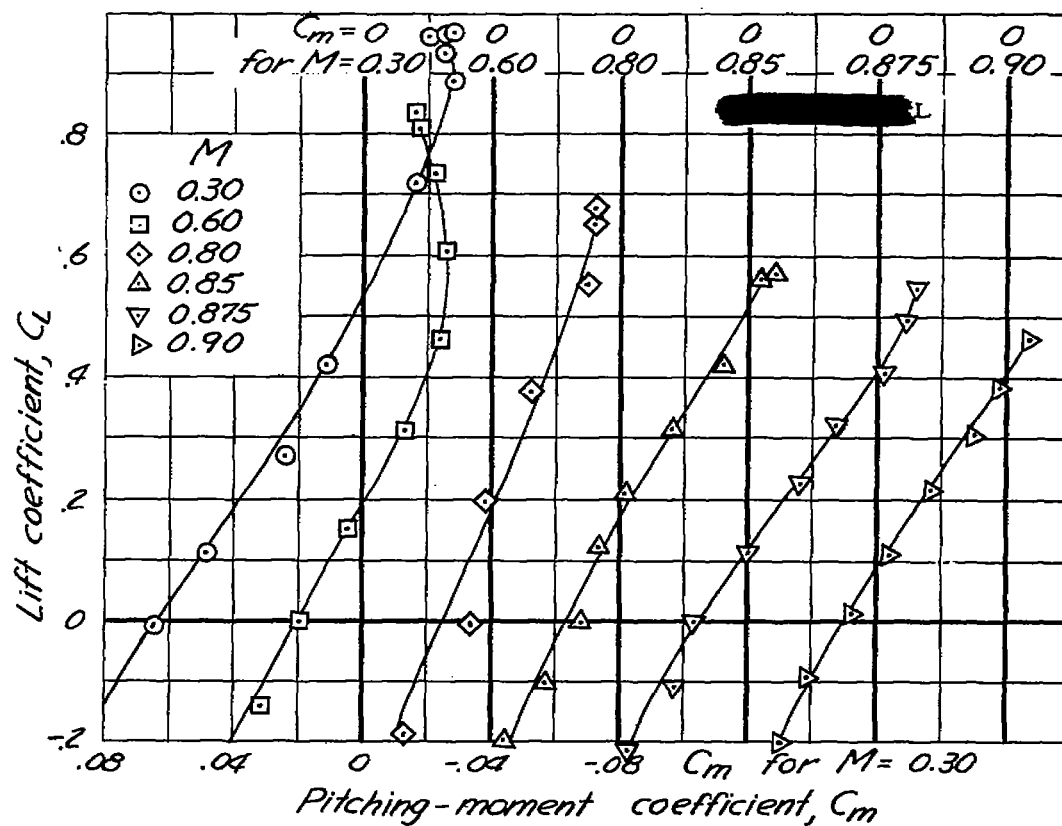


Figure 7.- Pitching-moment characteristics of the model without horizontal tail

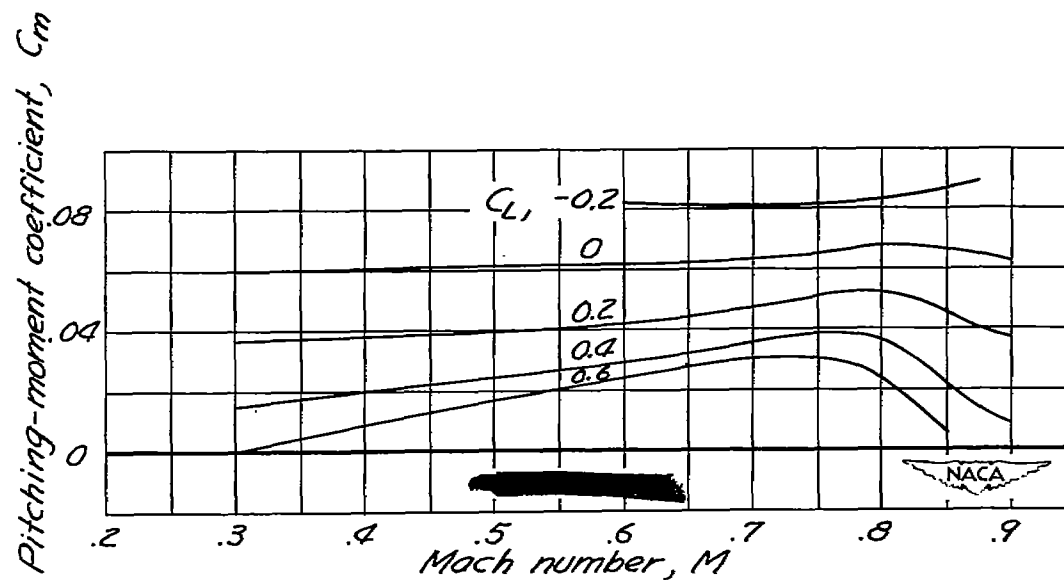
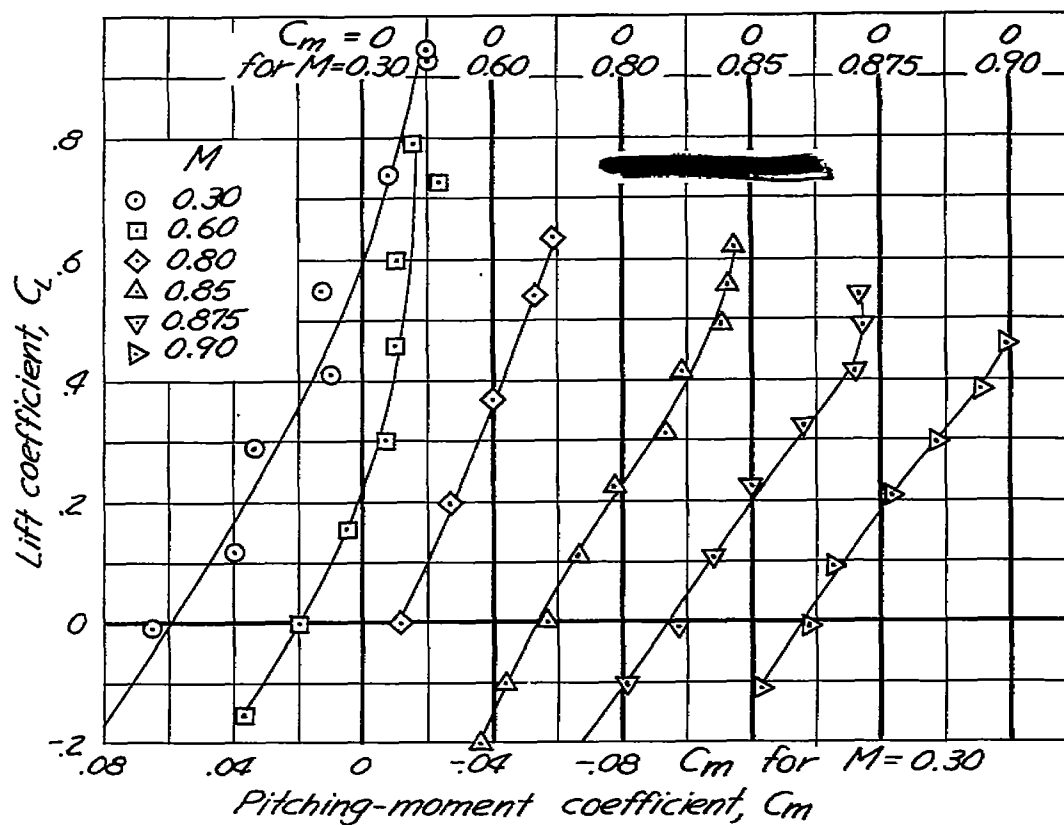


(a) Stabilizer and elevator neutral

Figure 8.- Pitching-moment characteristics of the model with horizontal tail



(b) stabilizer neutral, elevator deflected -5°
 Figure 8. - (Continued)



(c) Stabilizer deflected -3° , elevator neutral

Figure 8.- (Concluded)

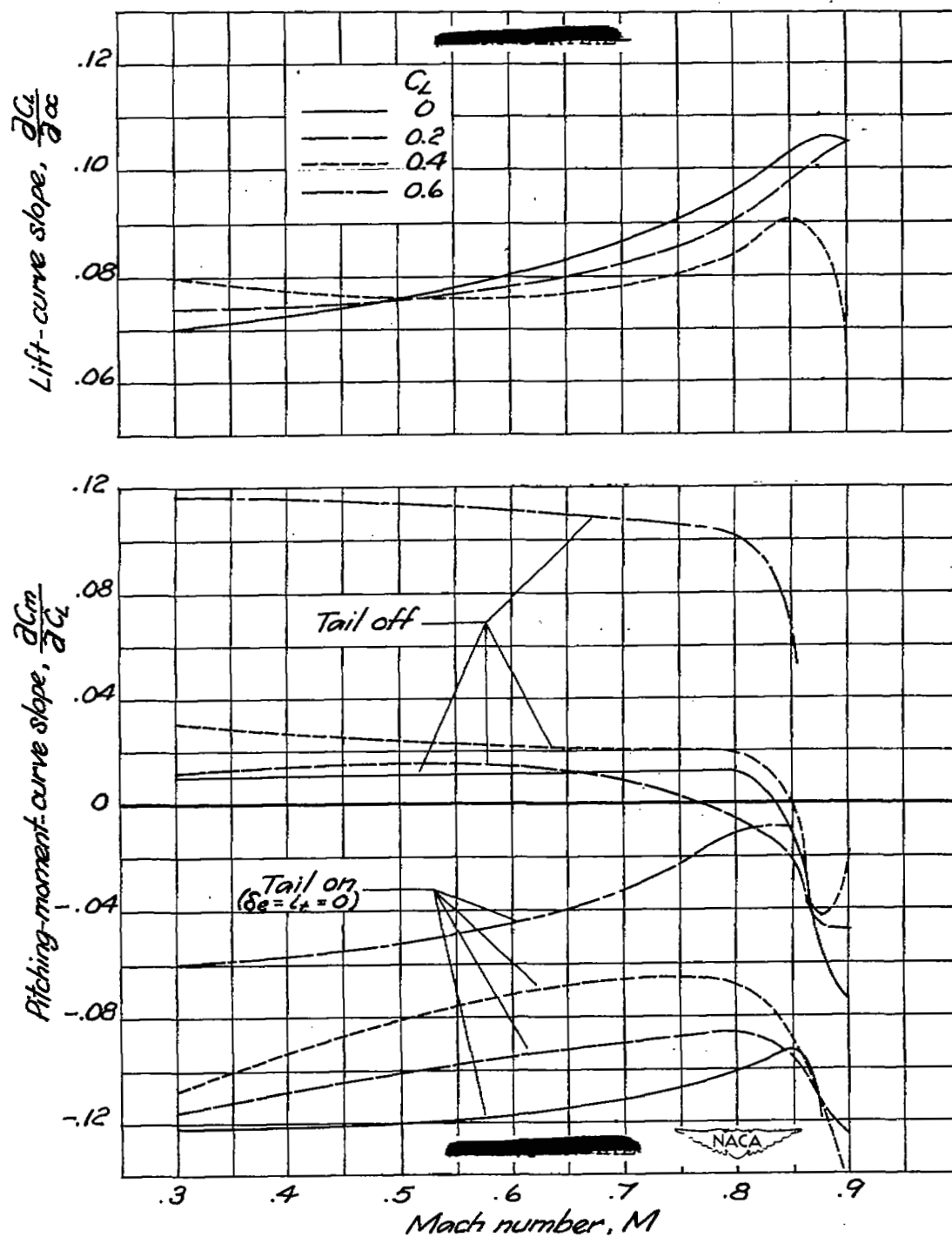


Figure 9. - Variation of lift-curve and pitching-moment-curve slopes with Mach number

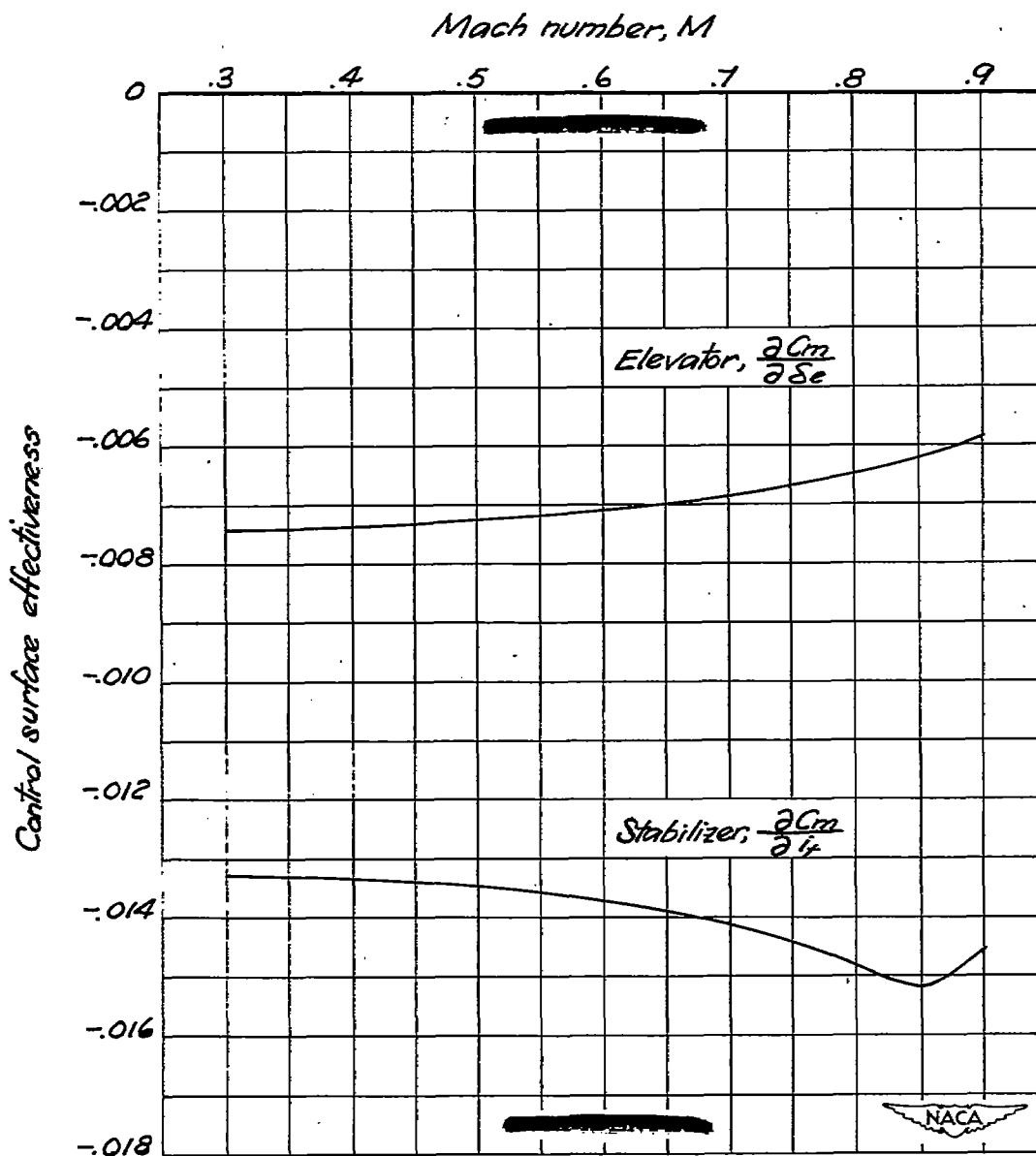
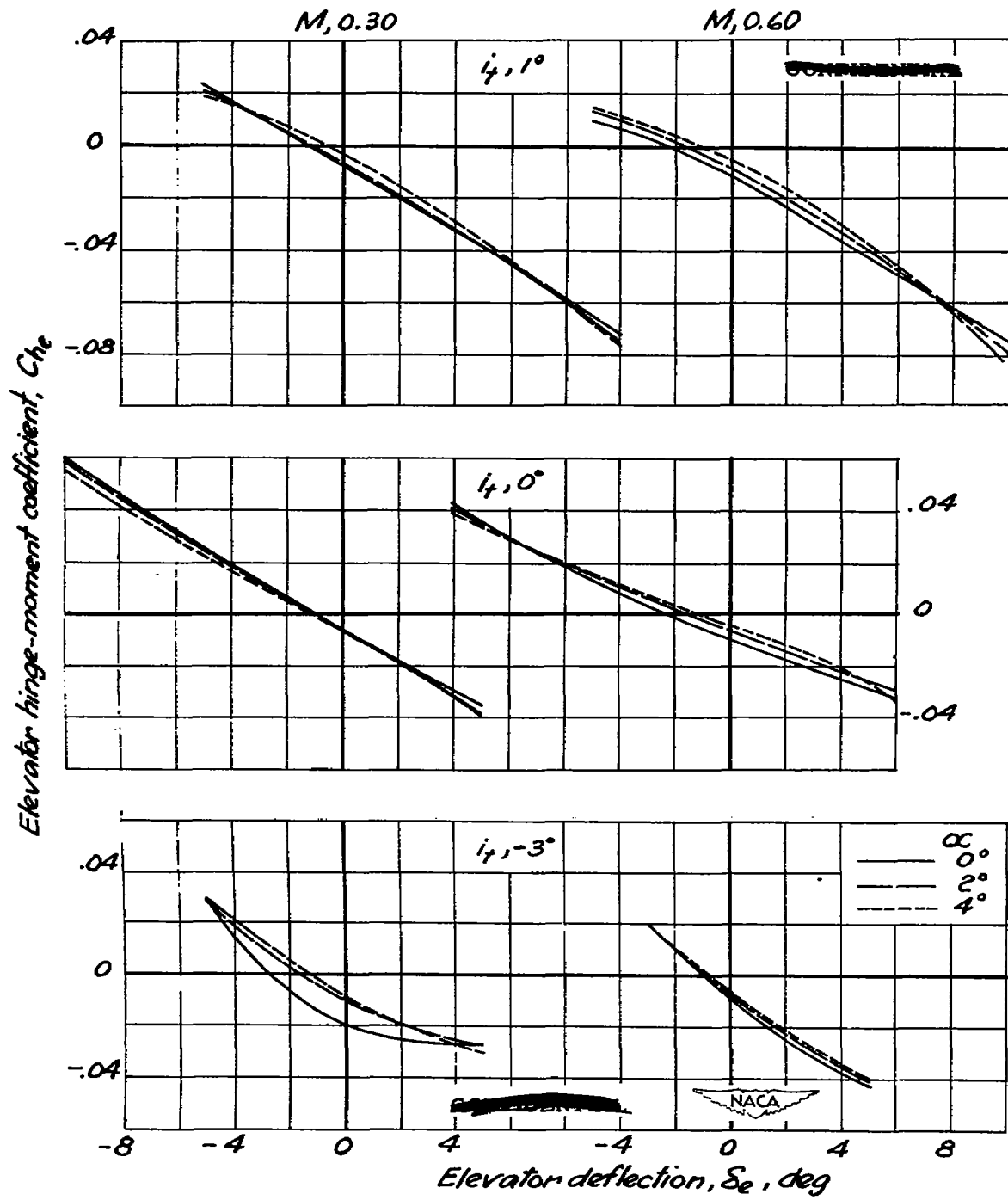


Figure 10.- Elevator effectiveness with zero stabilizer incidence and stabilizer effectiveness with zero elevator deflection; $C_L, 0$



(a) $M, 0.30, 0.60$

Figure 11.- Elevator hinge-moment characteristics

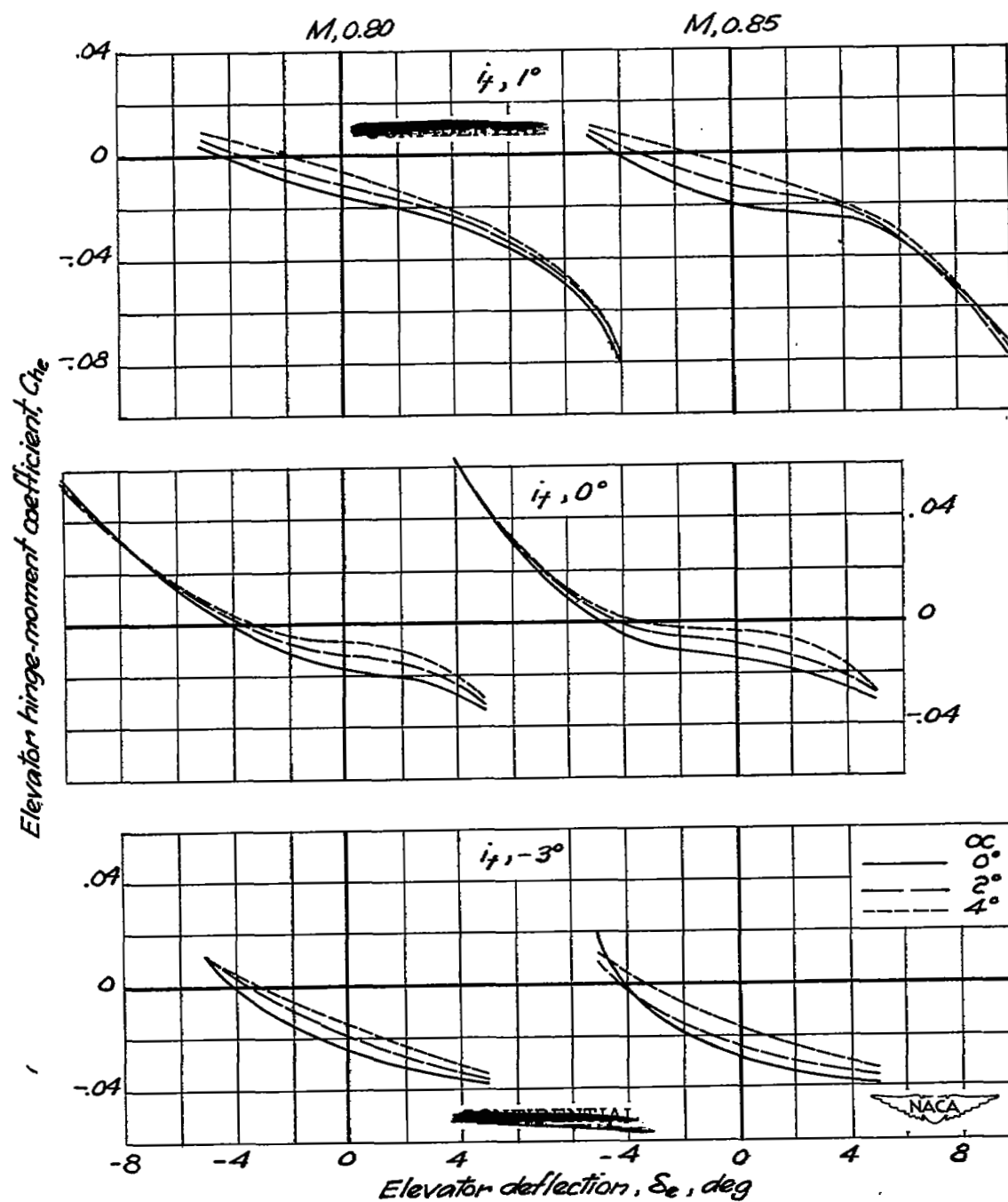
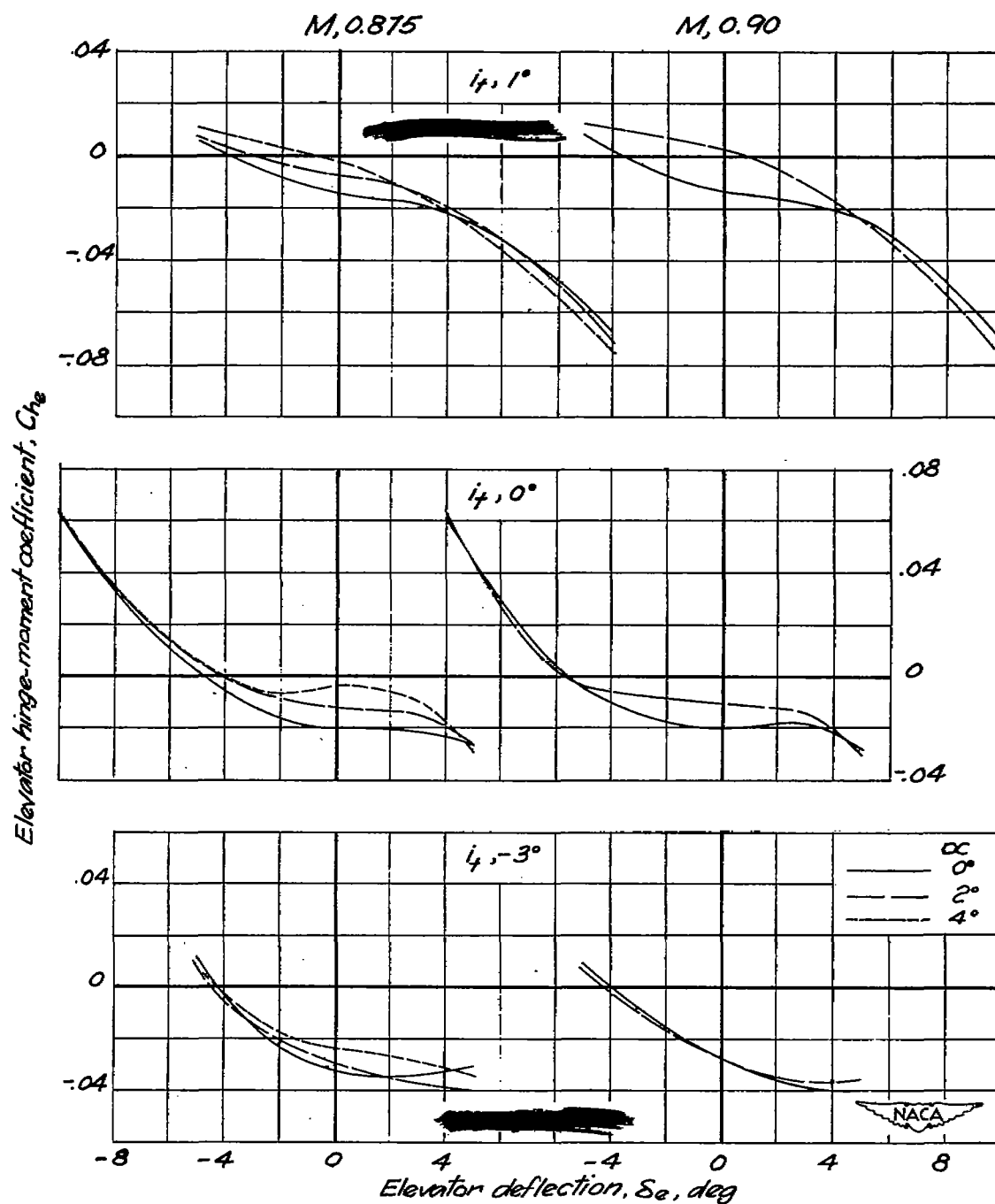
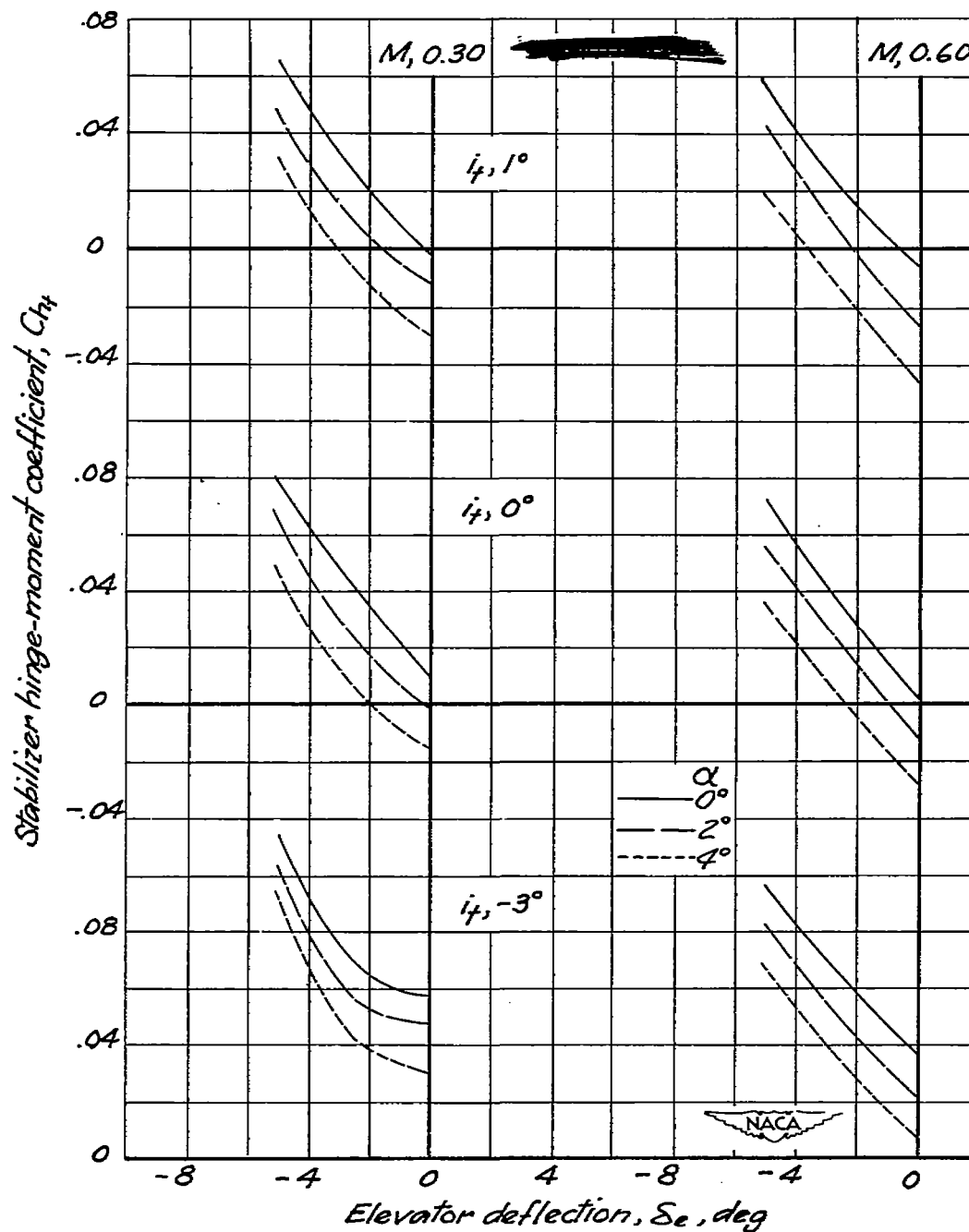
(b) $M, 0.80, 0.85$

Figure 11.-(Continued)



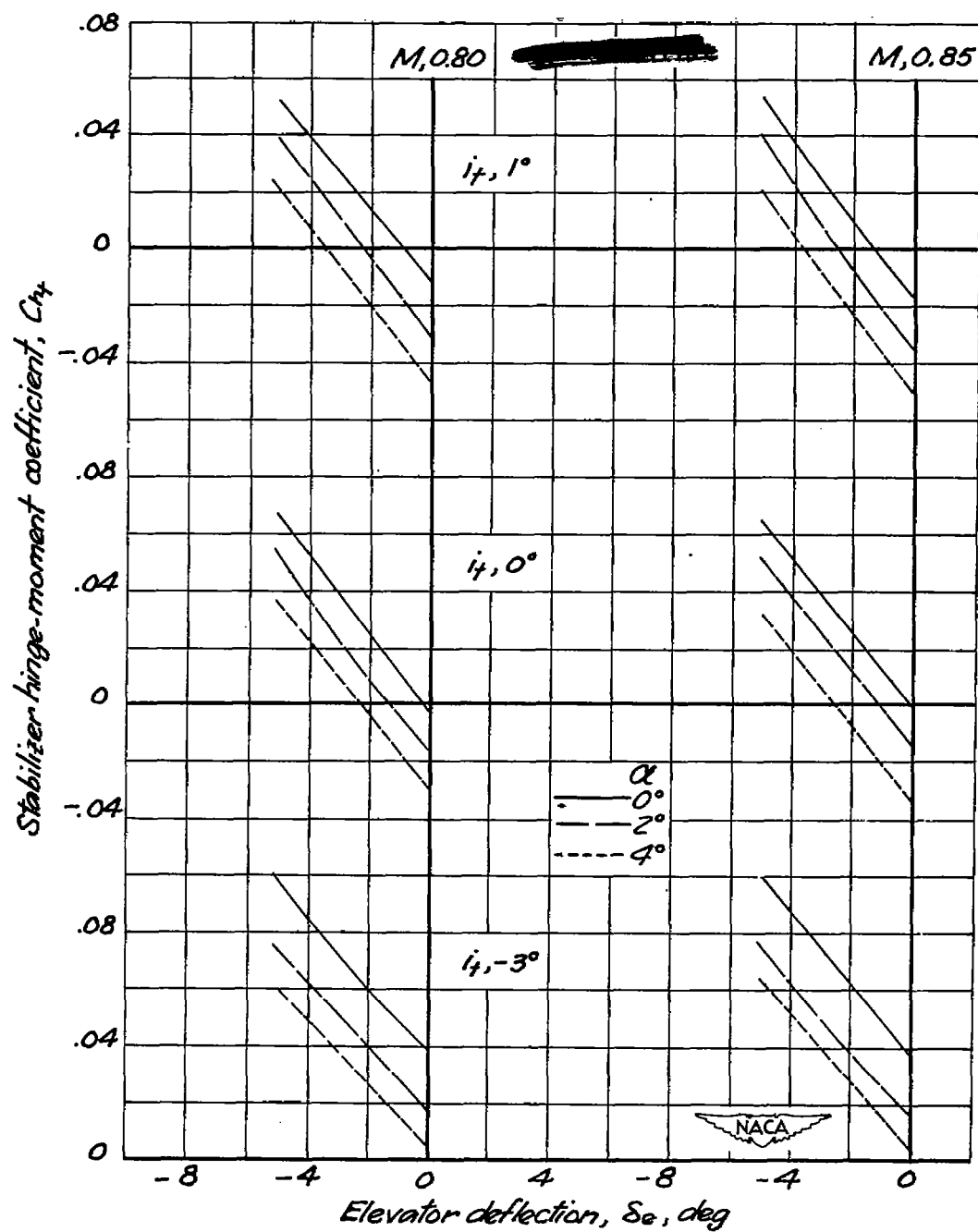
(c) $M, 0.875, 0.90$

Figure 11. - (Concluded)



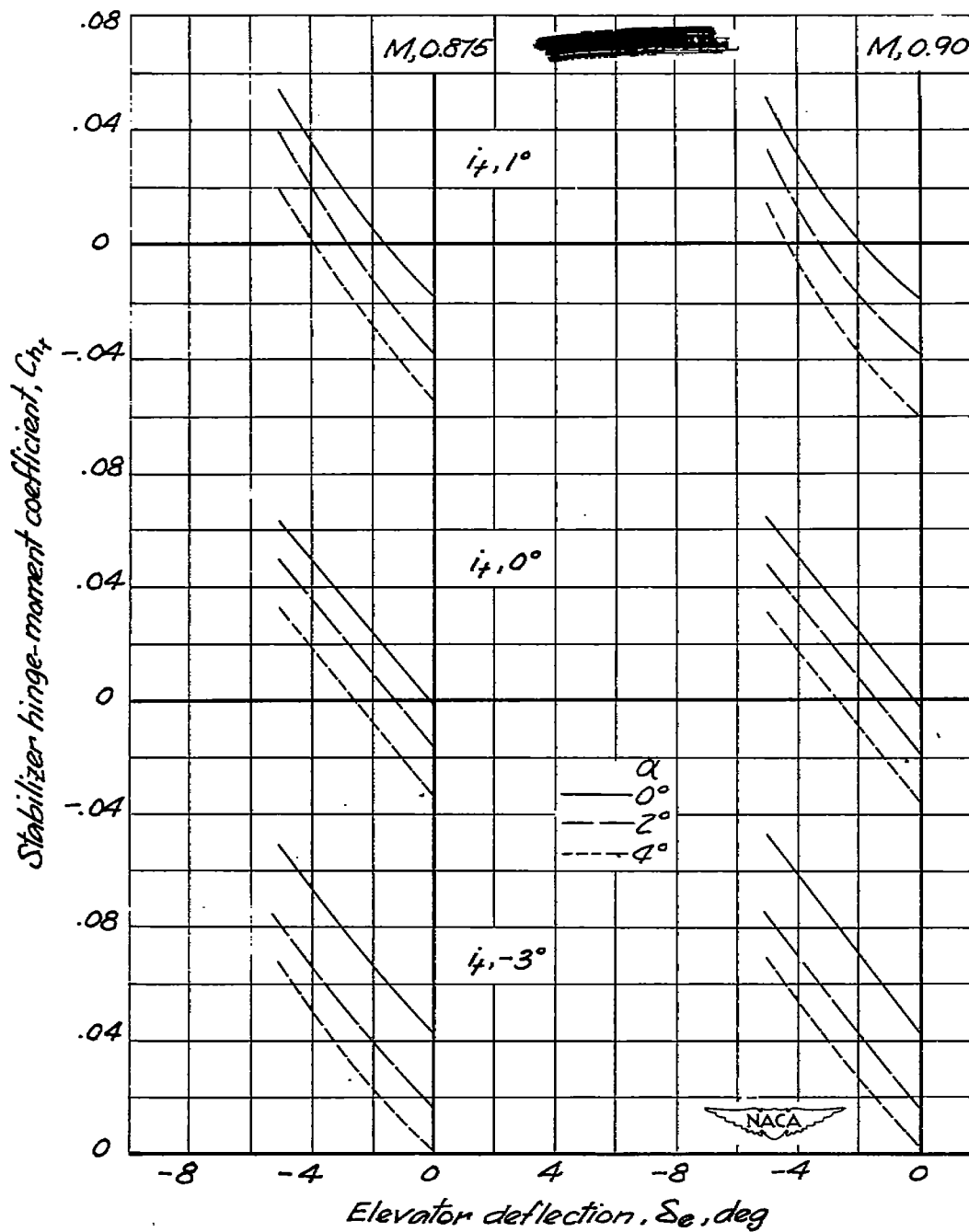
(a) $M, 0.30, 0.60$

Figure 12.- Variation of stabilizer hinge-moment coefficient with elevator deflection



(b) $M, 0.80, 0.85$

Figure 12.- (Continued)



(c) $M_0.875, 0.90$

Figure 12. - (Concluded)

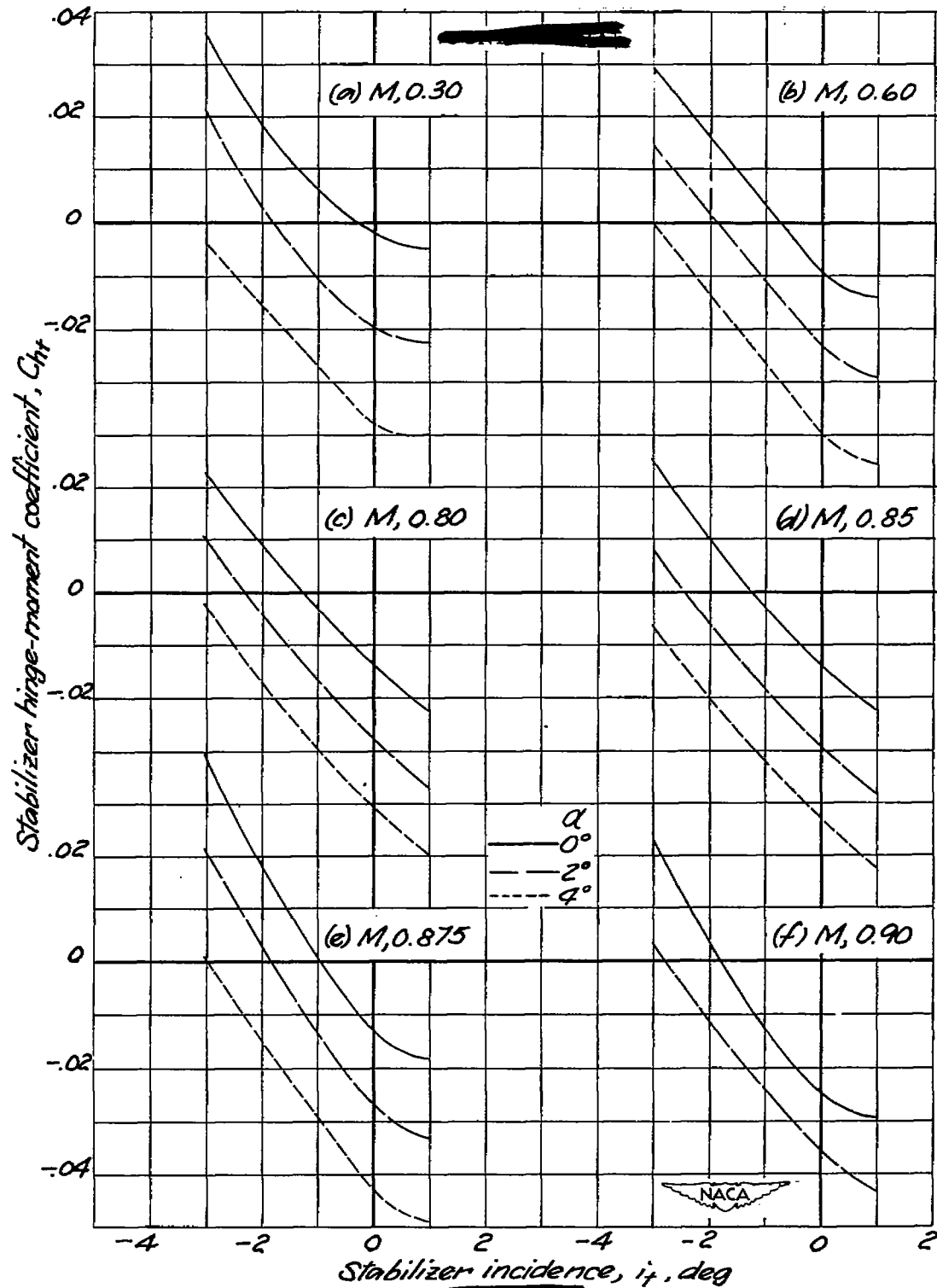


Figure 13.- Stabilizer hinge-moment characteristics

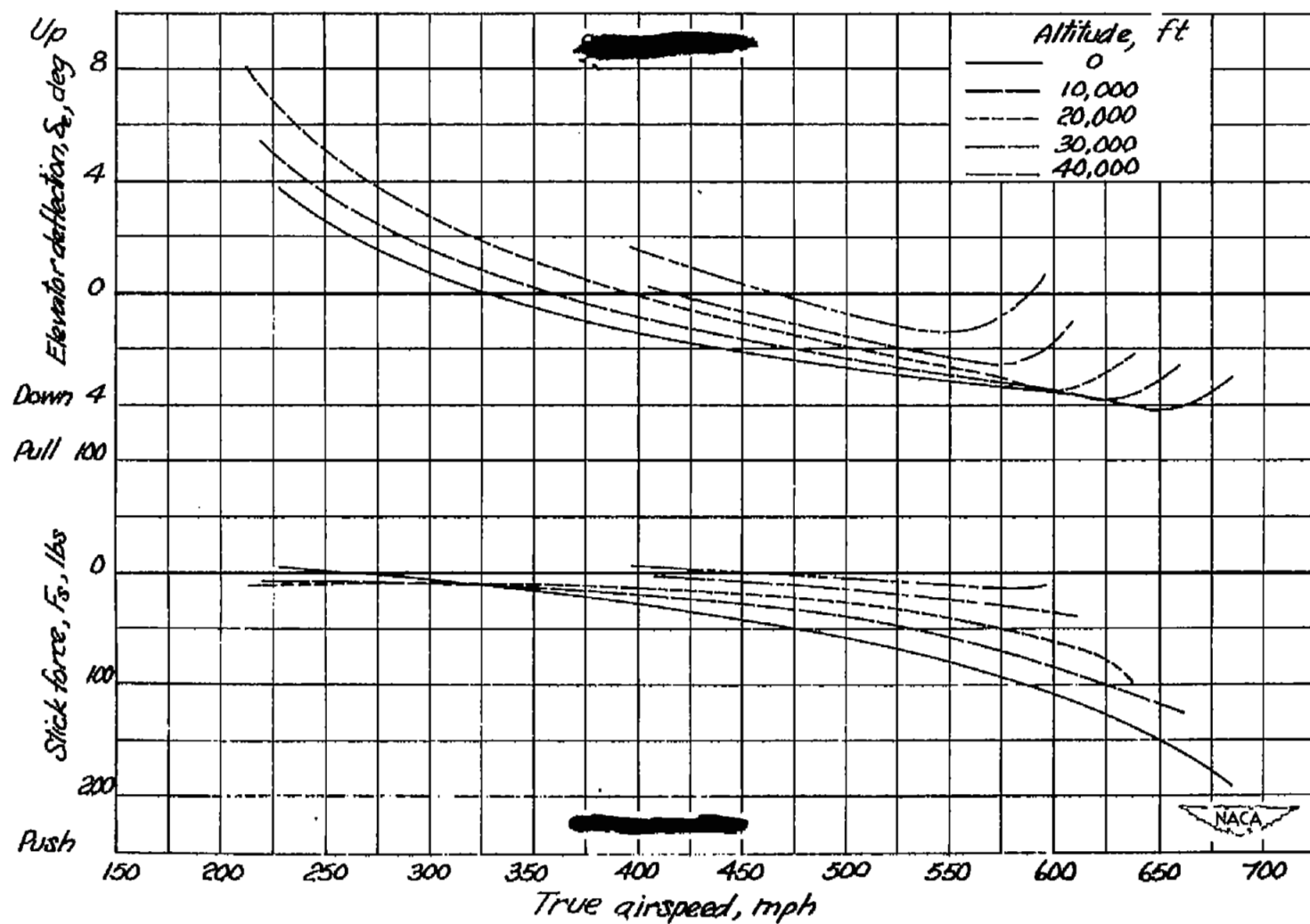


Figure 14.- Variation with airspeed of elevator deflection and stick force for level flight

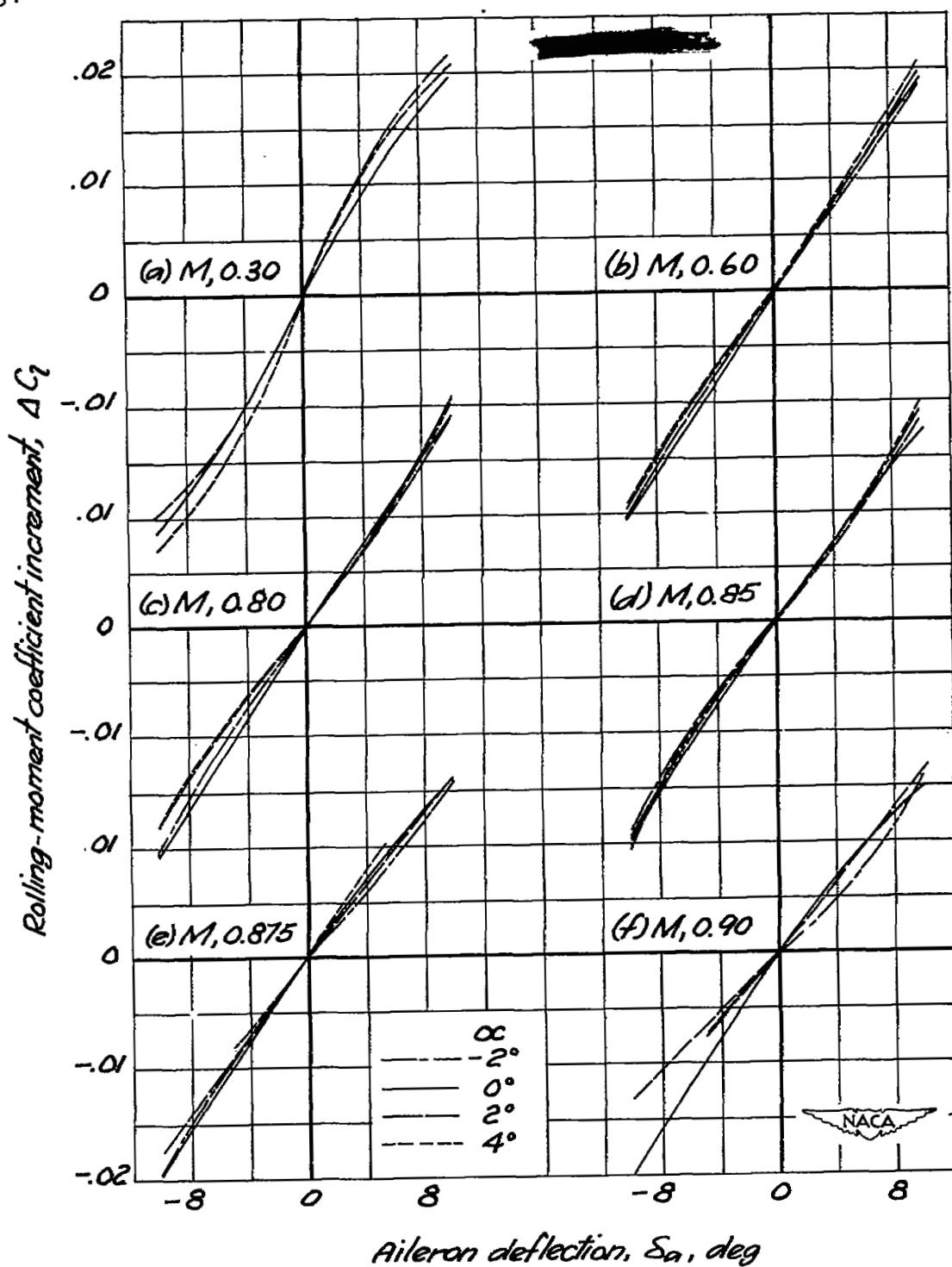


Figure 15.- Aileron effectiveness

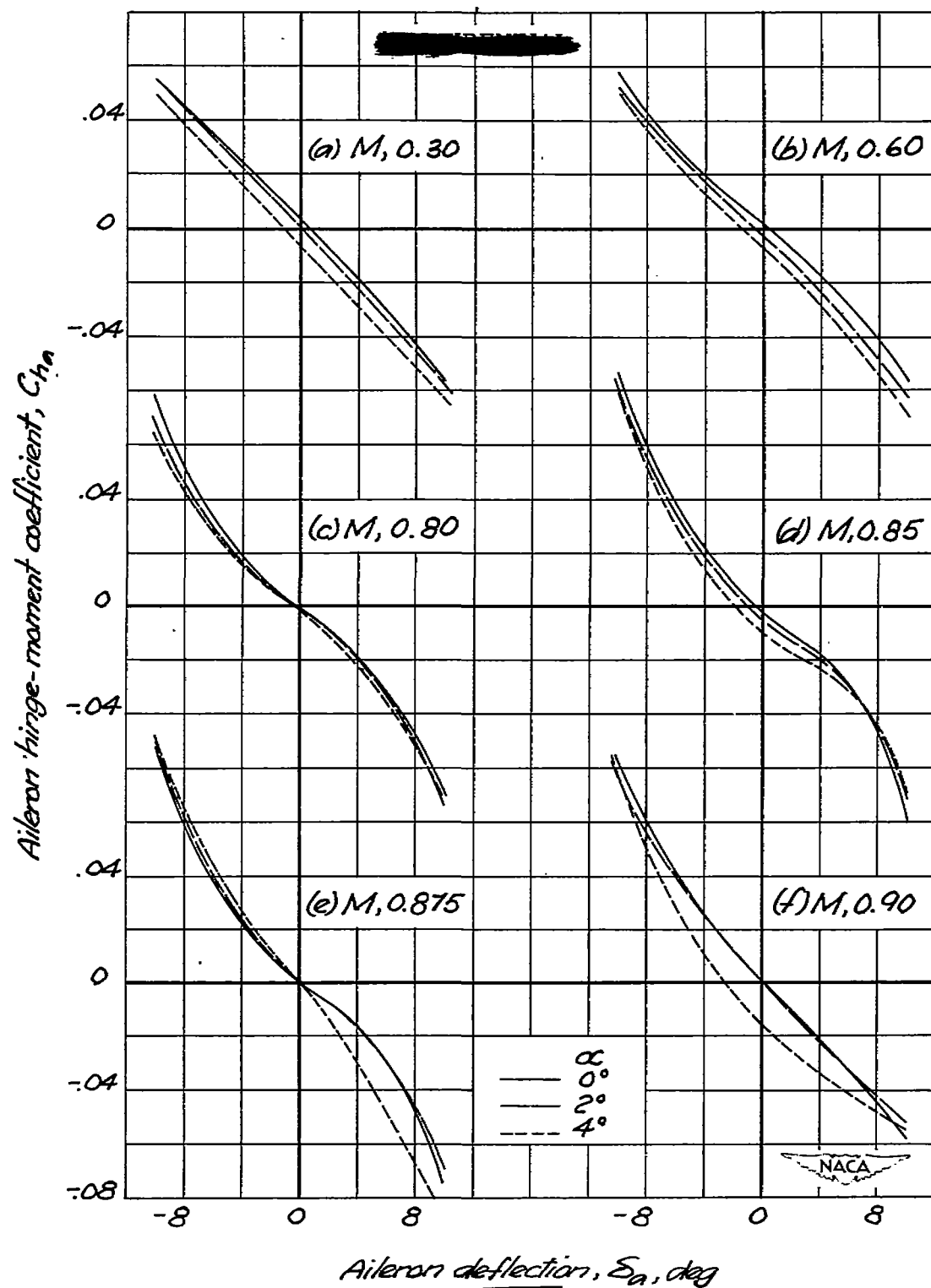


Figure 16.- Aileron hinge-moment characteristics

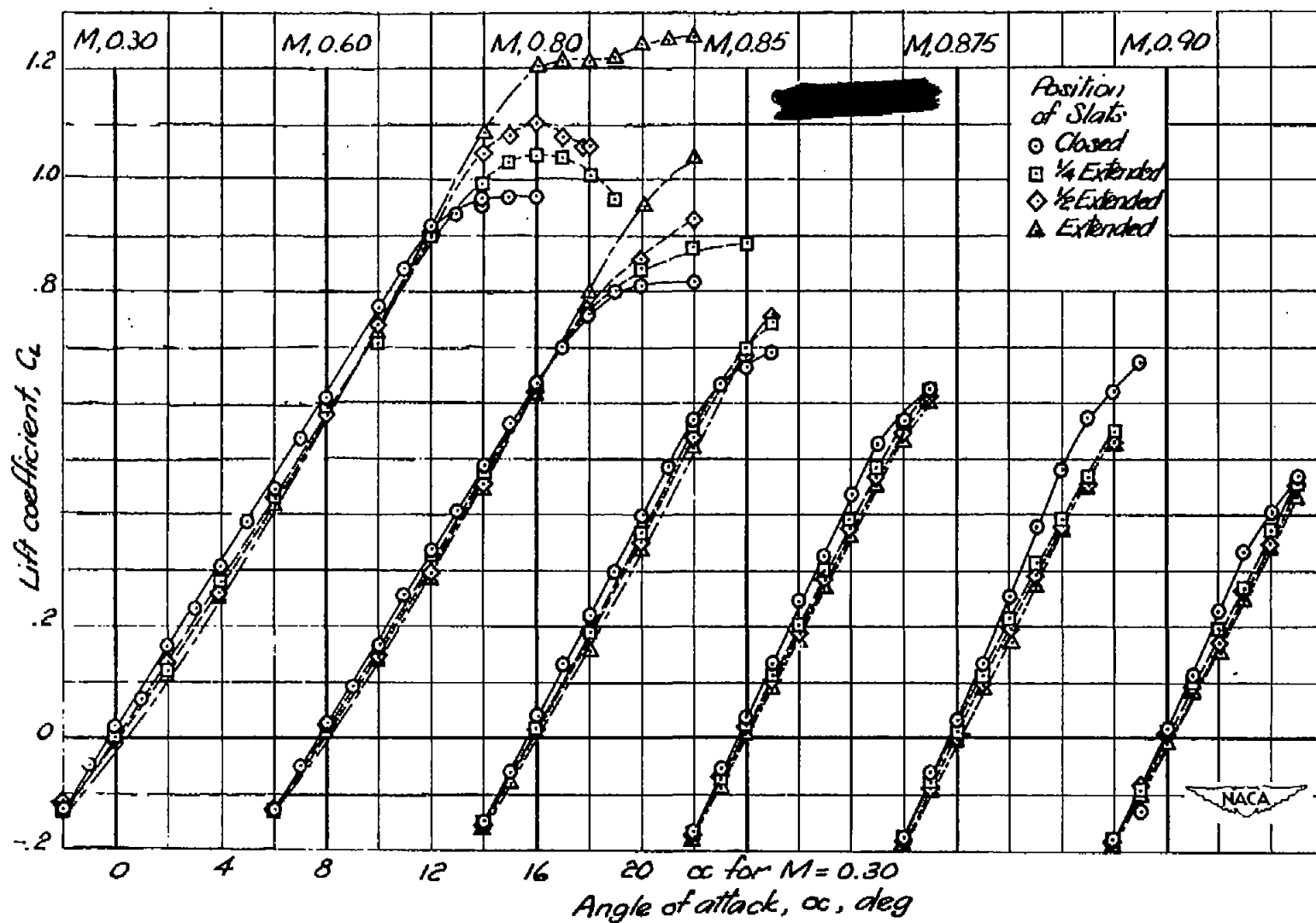


Figure 17.- Lift characteristics with closed and extended slats

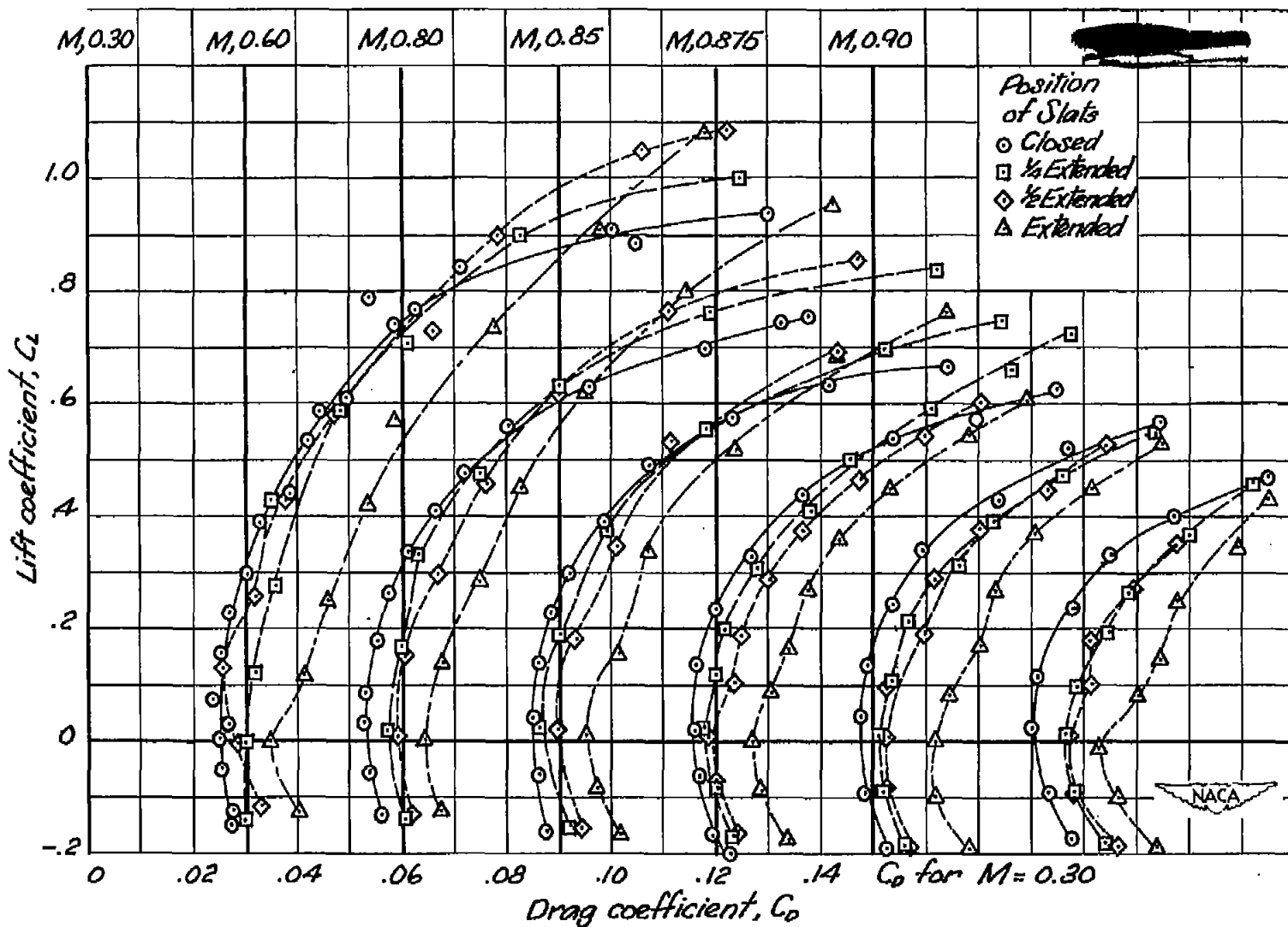


Figure 18.- Drag characteristics with closed and extended slats

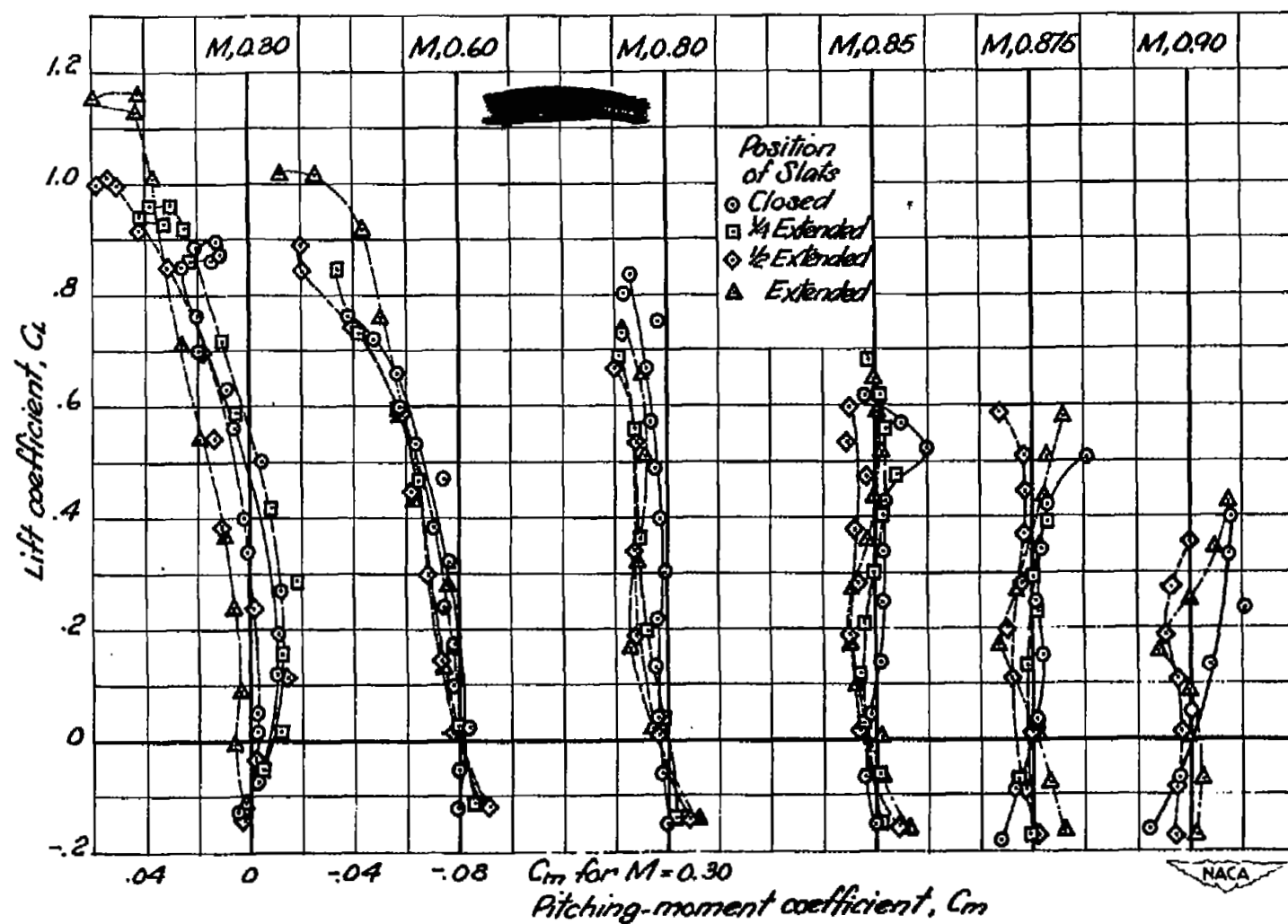


Figure 19.- Tail-off pitching-moment characteristics with closed and extended slats

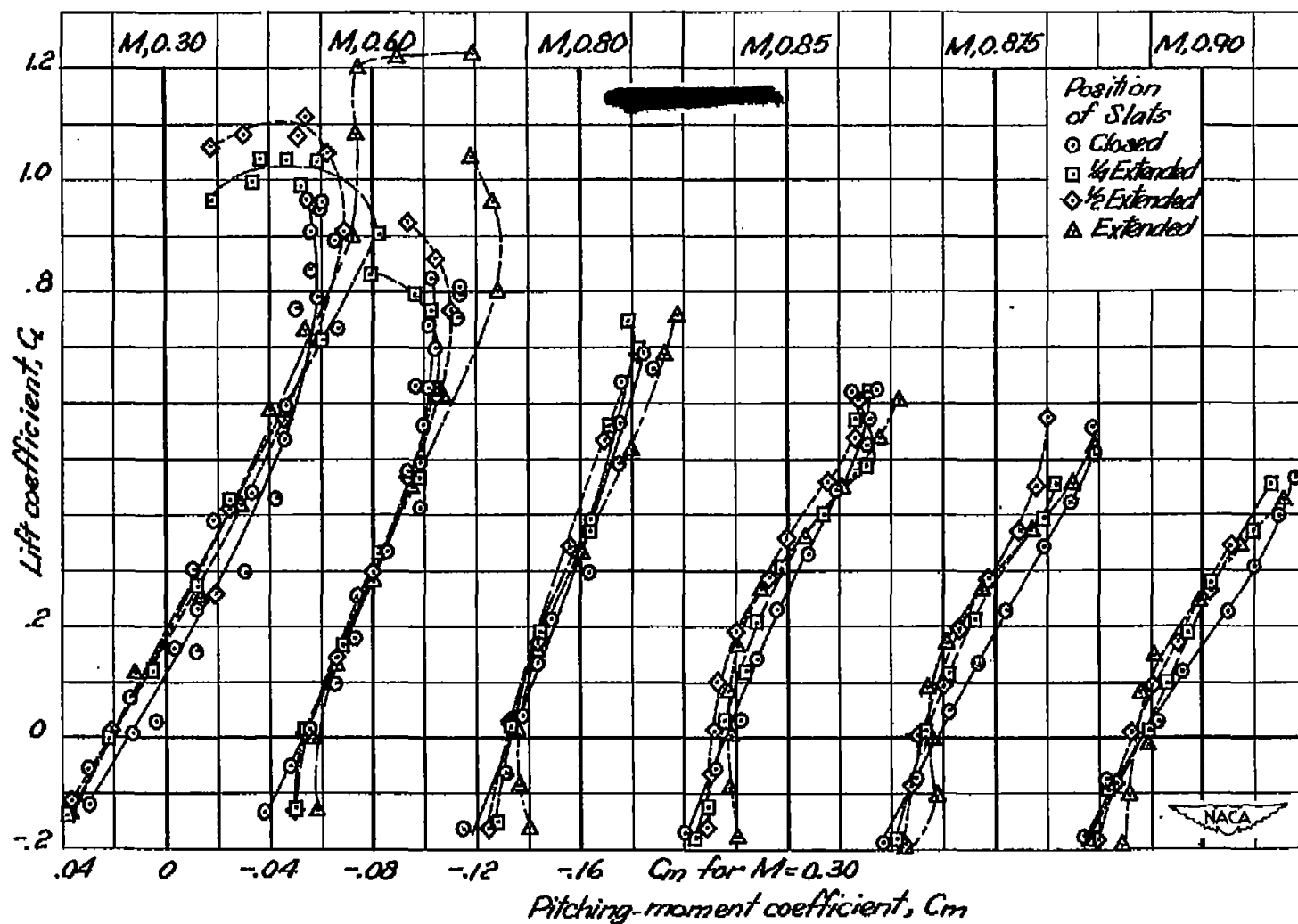


Figure 20.- Tail-on pitching-moment characteristics with closed and extended slats

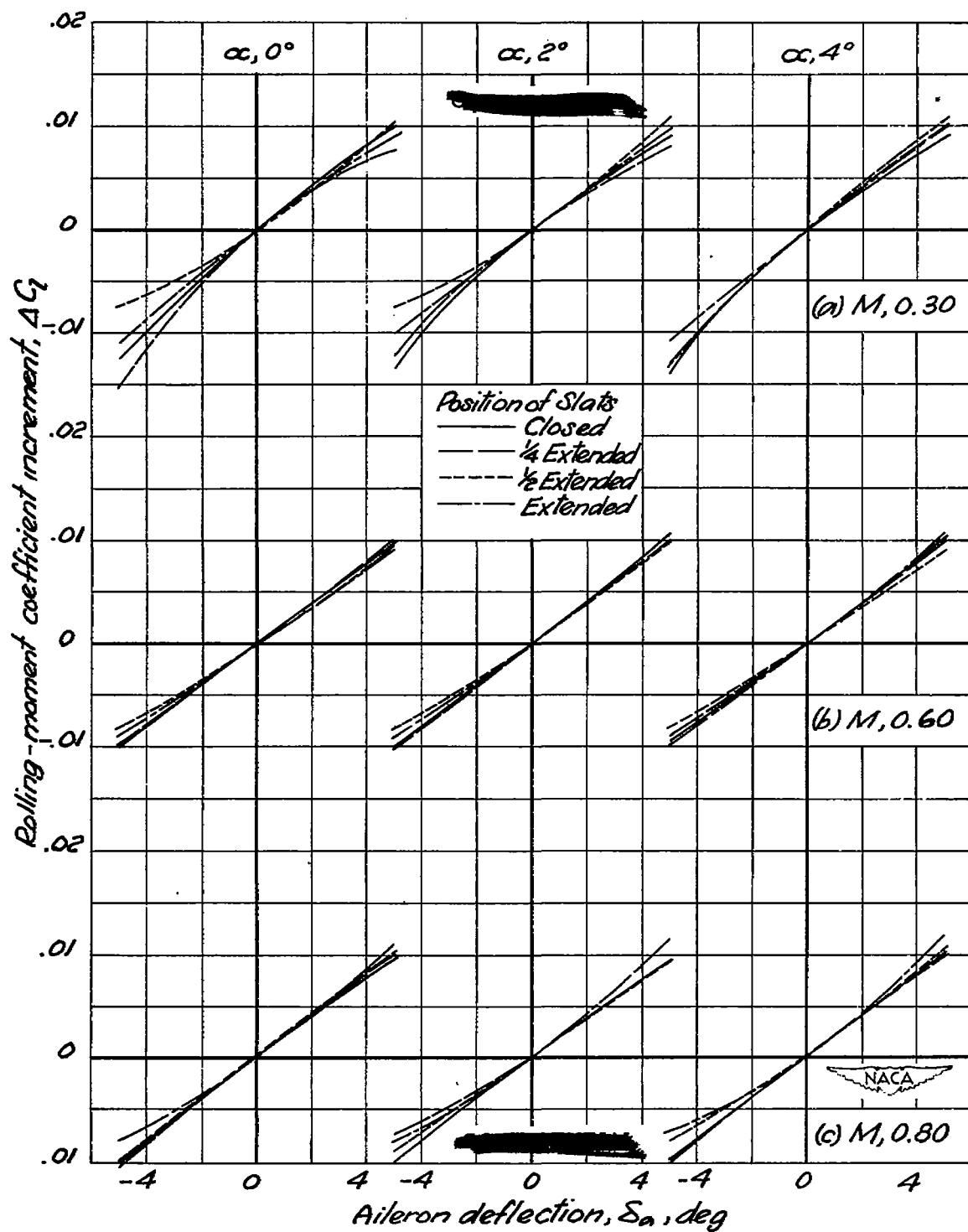


Figure 21.- Aileron characteristics with closed and extended slats

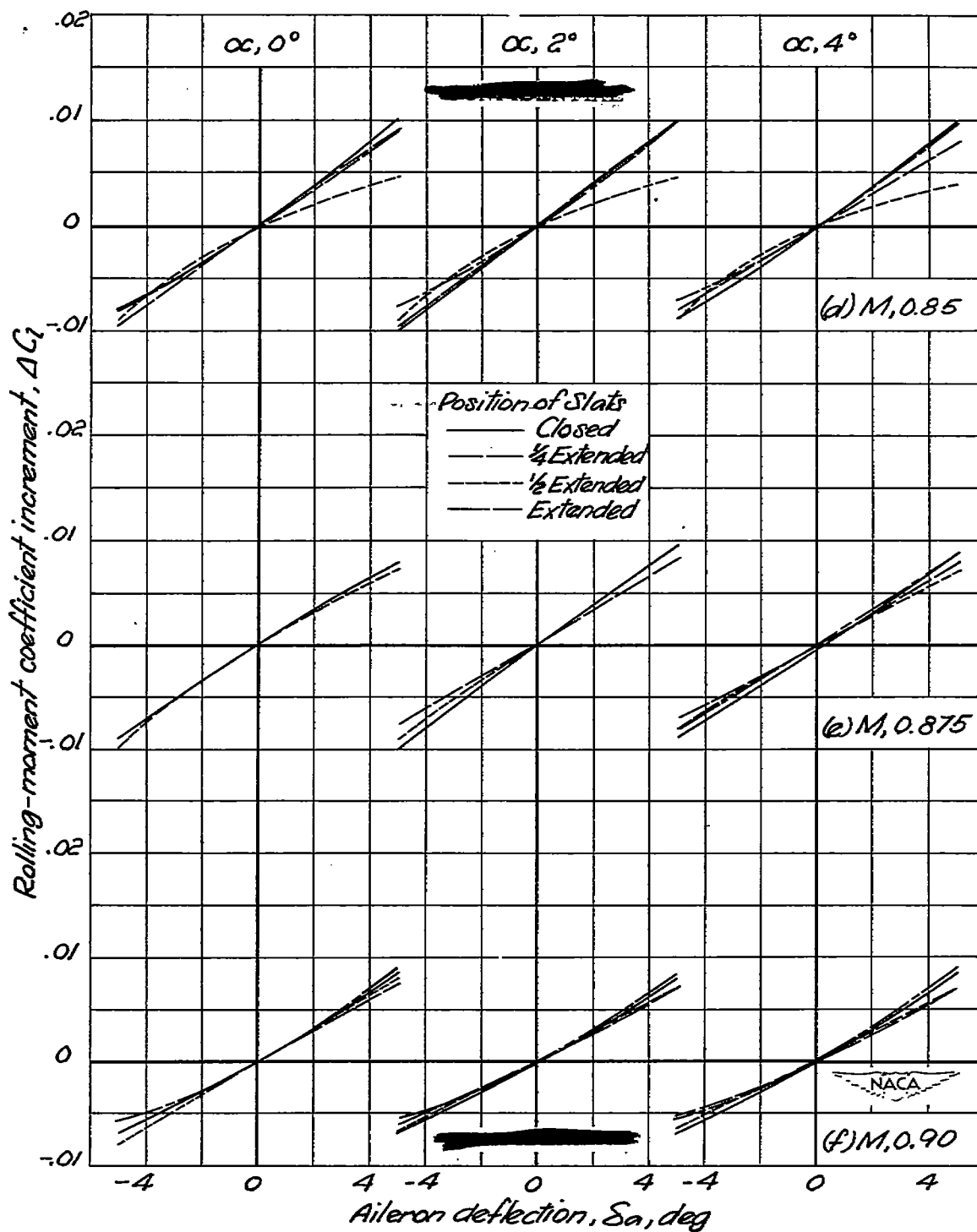


Figure 21.- (Concluded)

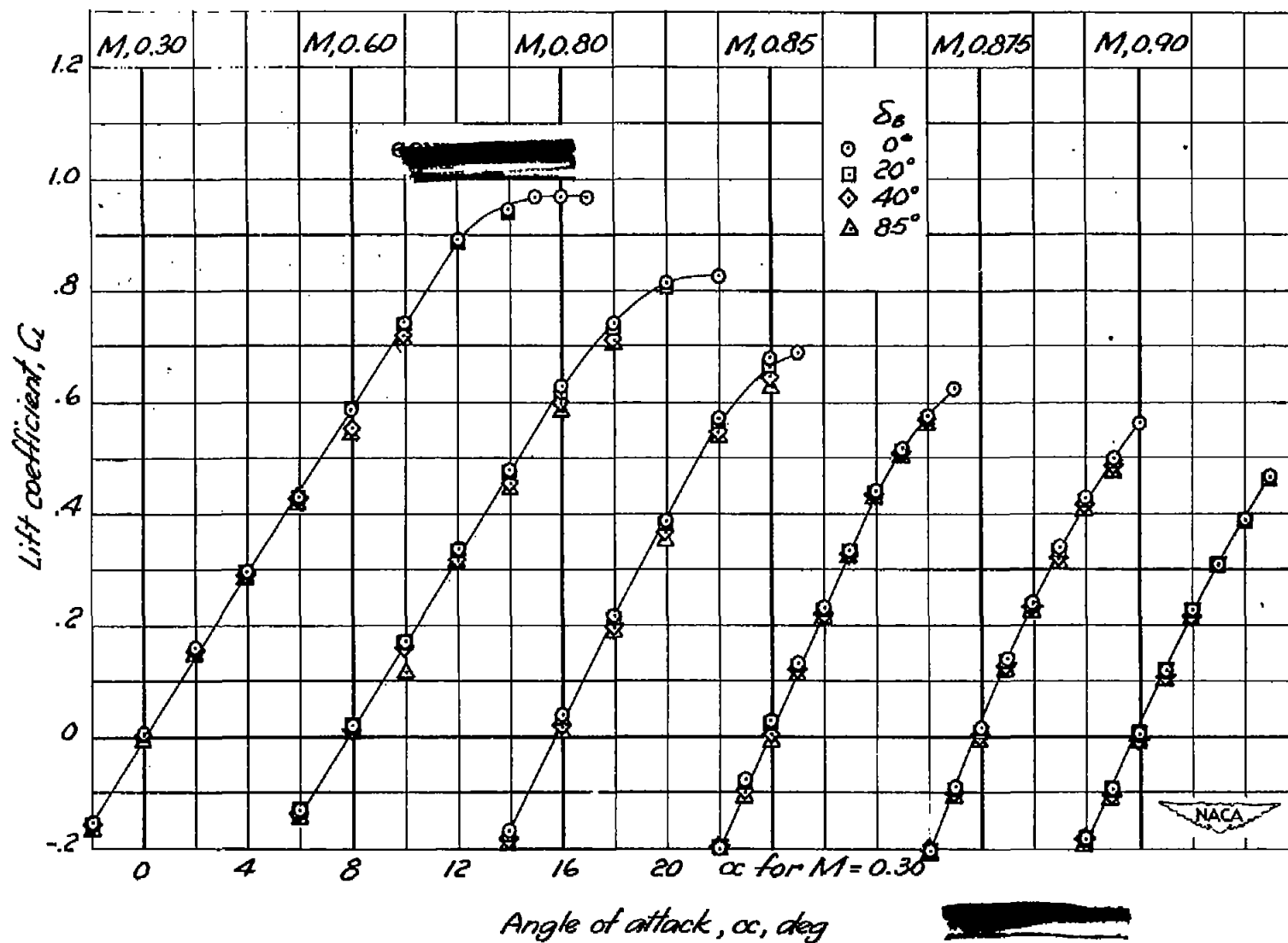
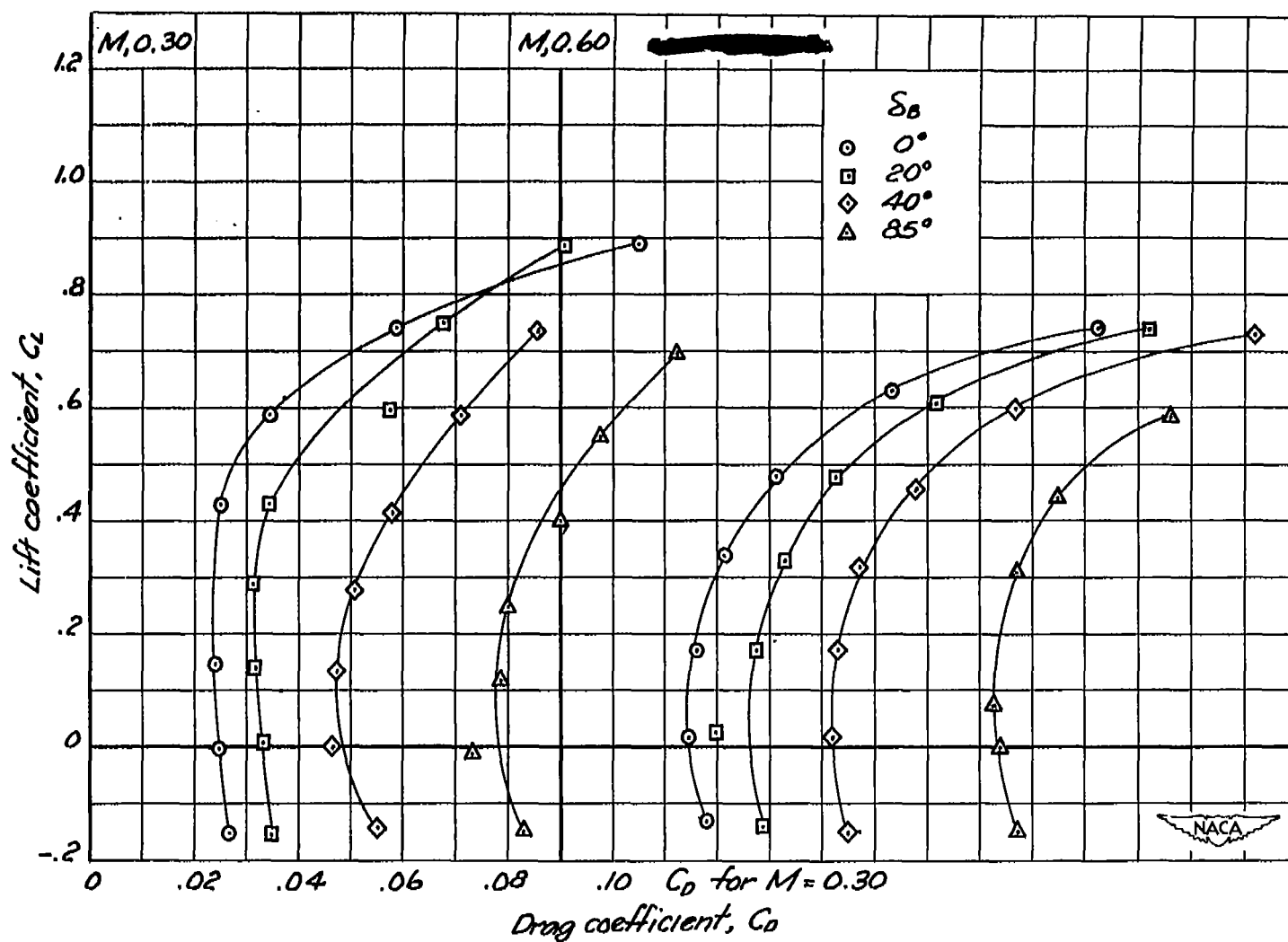
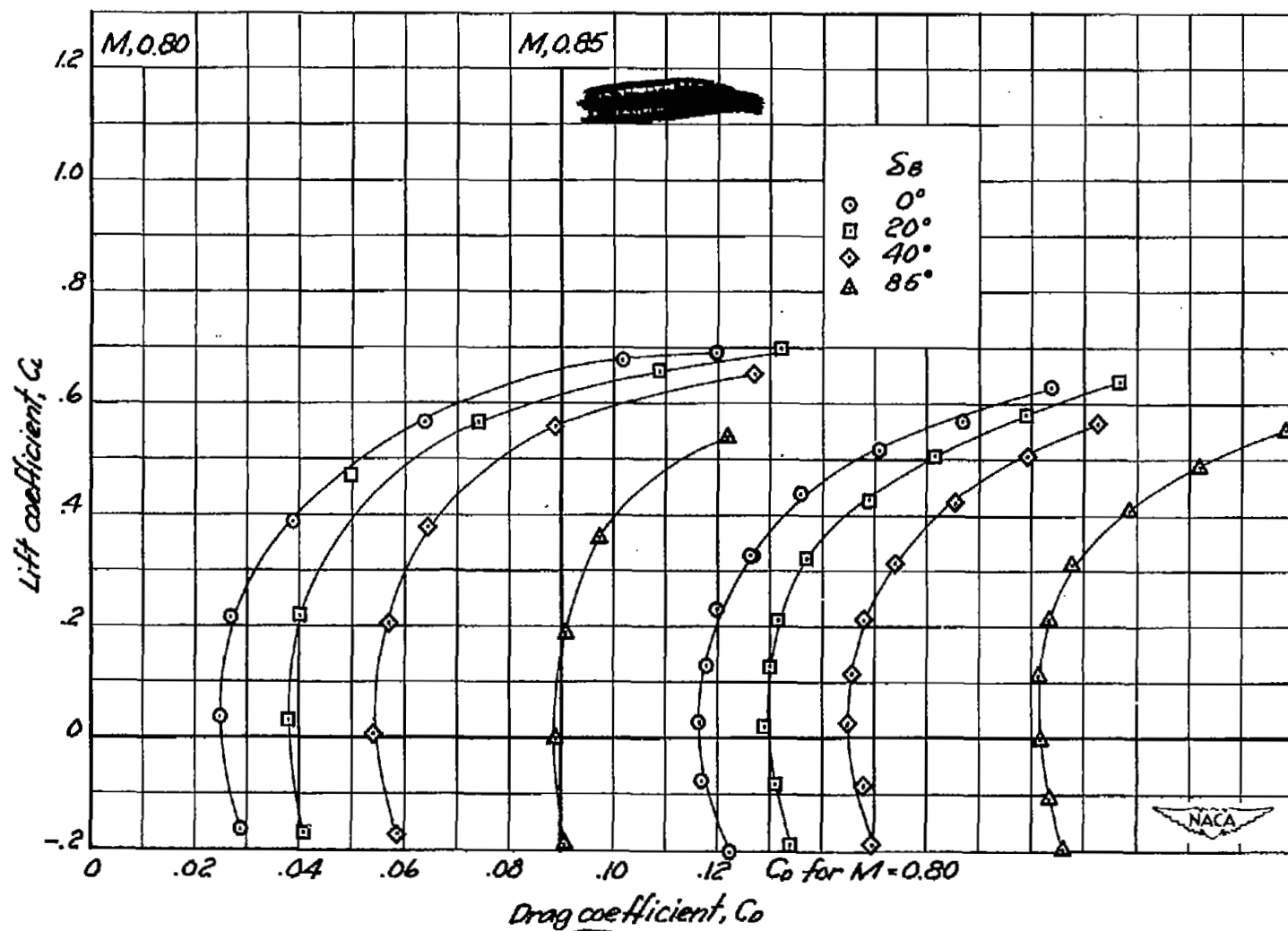


Figure 22.-Lift characteristics with dive brake closed and deflected

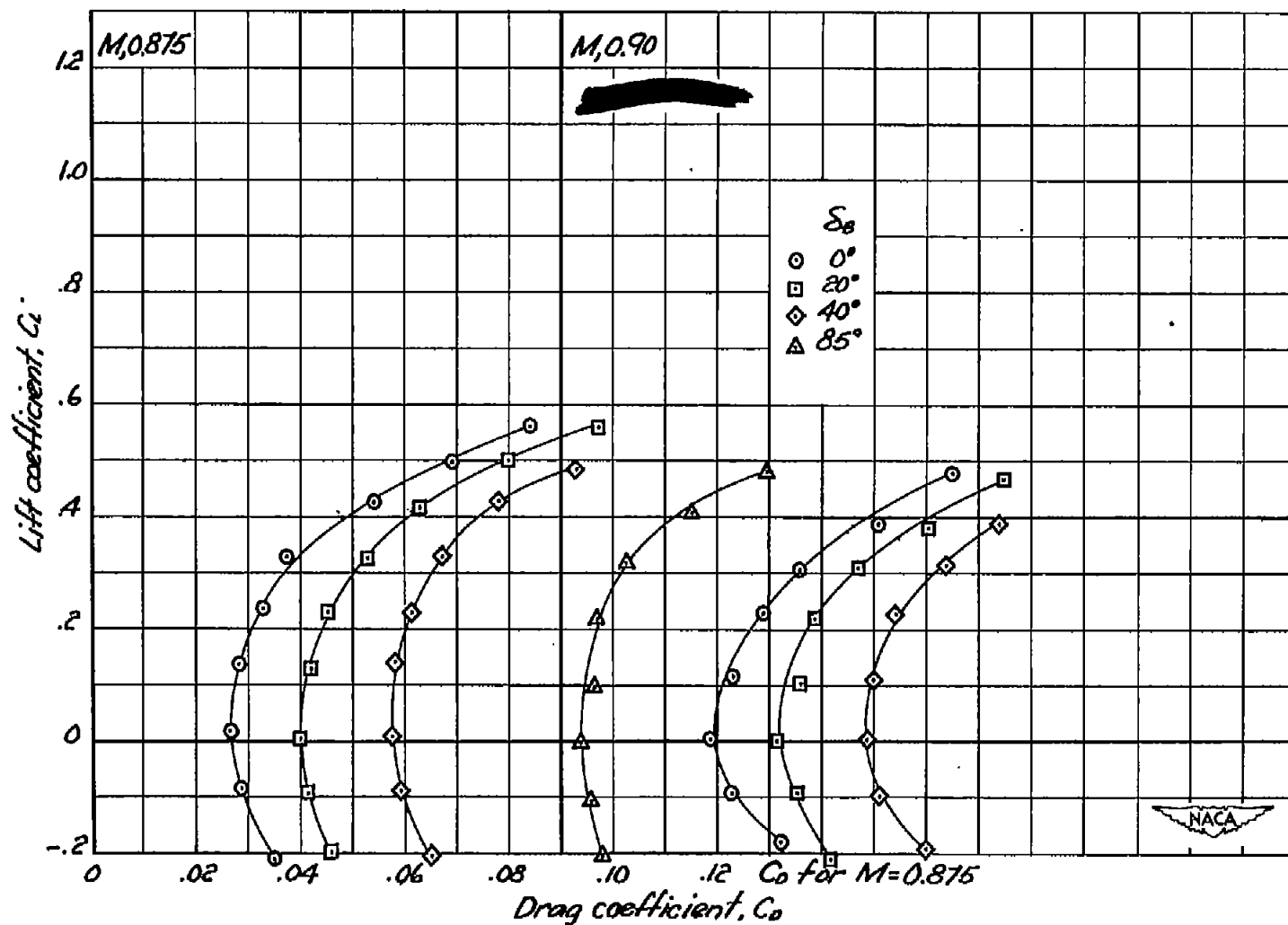


(a) $M, 0.30, 0.60$

Figure 23.- Drag characteristics with the dive brake closed and deflected



(b) $M, 0.80, 0.85$
Figure 23. - (Continued)



(c) $M, 0.875, 0.90$
Figure 23.- (concluded)

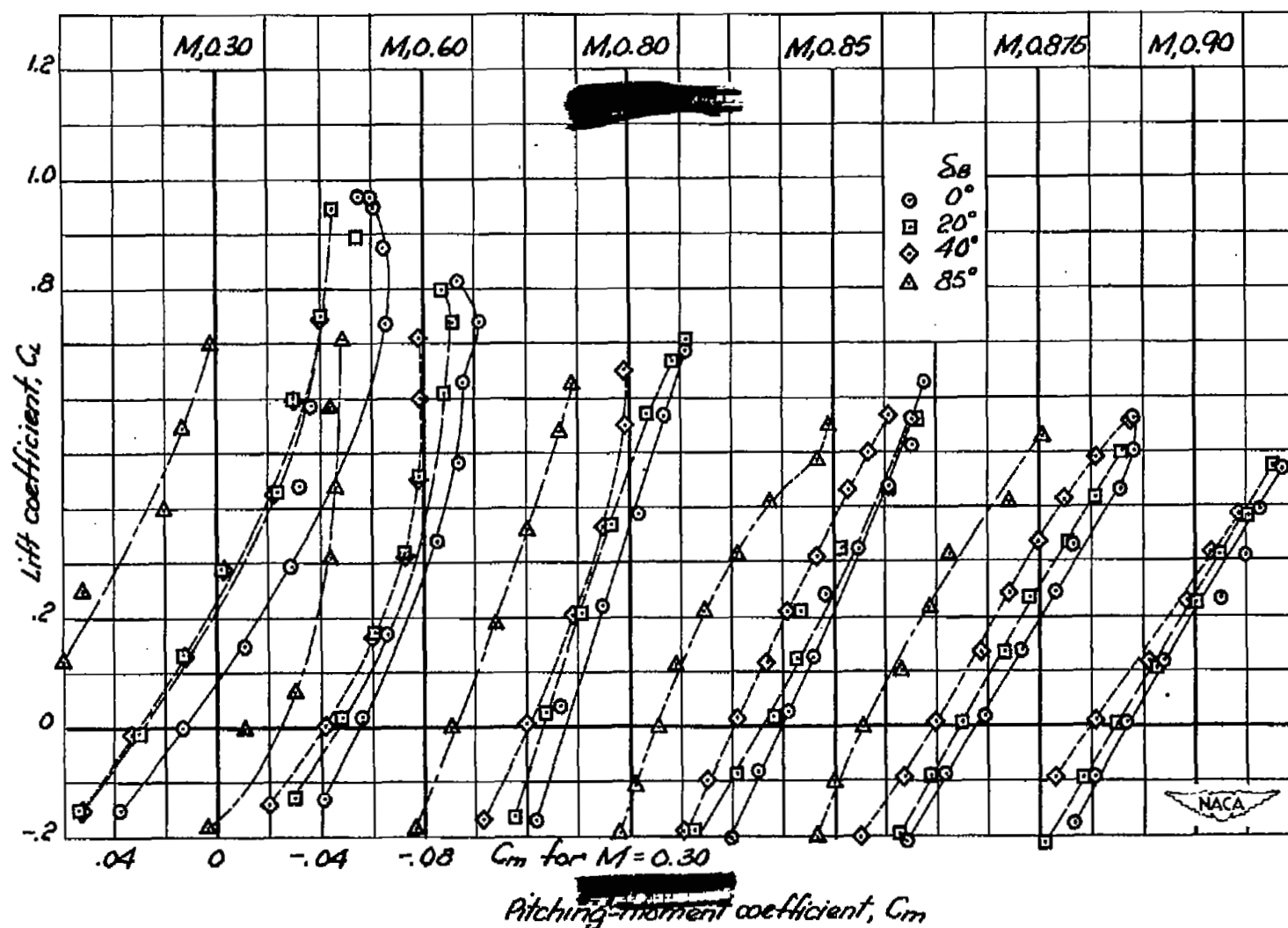


Figure 24.- Pitching-moment characteristics with the dive brake closed and deflected

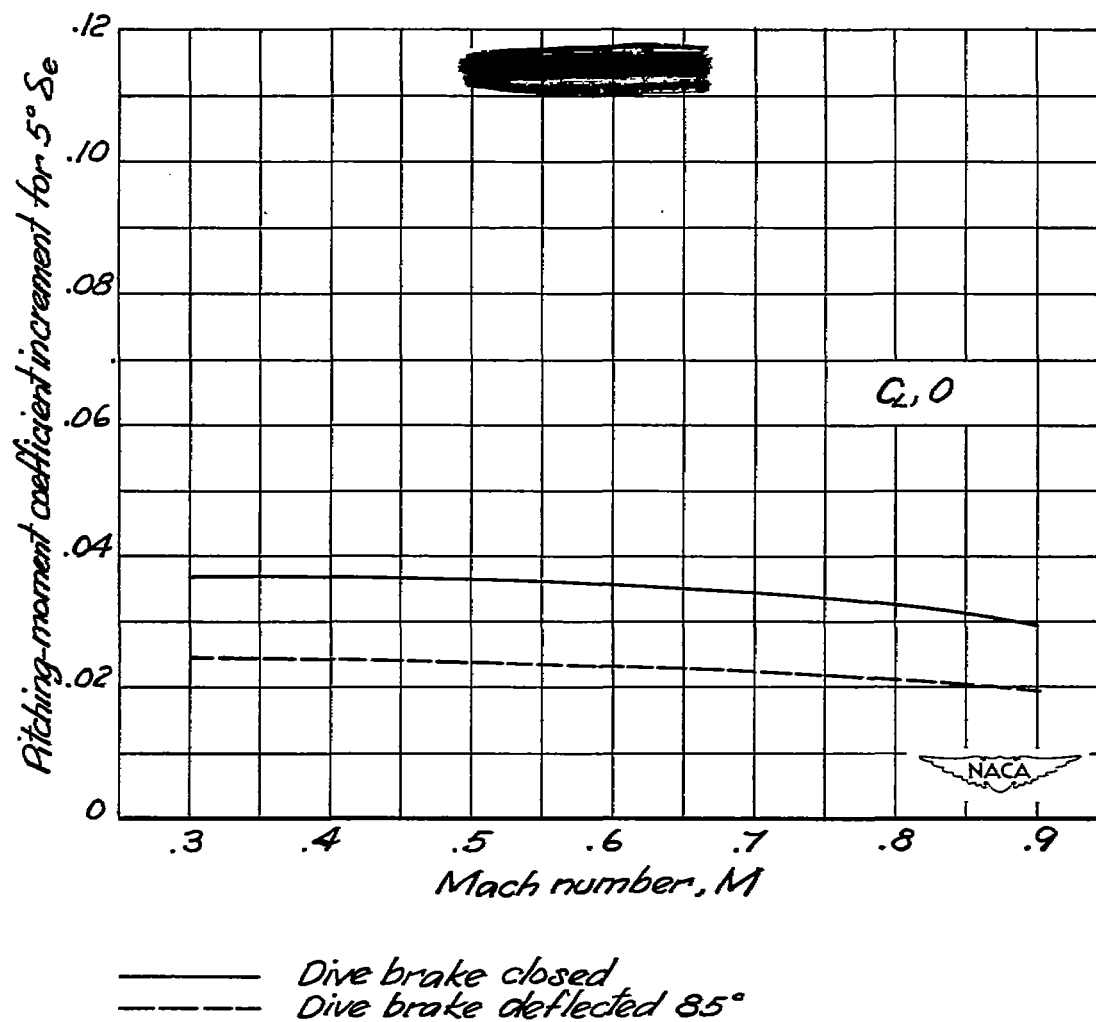


Figure 25.- Elevator effectiveness with dive brake closed and deflected

NASA Technical Library



3 1176 01434 4452